Impacts of future climate and land cover changes on landslide susceptibility: Regional scale modelling in the Val d'Aran region (Pyrenees, Spain)

Marcel Hürlimann (1), Zizheng Guo (1, 2*), Carol Puig-Polo (1), Vicente Medina (1)

[1] *Division of Geotechnical Engineering and Geosciences; Department of Civil and Environmental Engineering, UPC BarcelonaTECH; 08034 Barcelona, Spain*

[2] *Department of Engineering Geology and Geotechnical Engineering, Faculty of Engineering, China University of Geosciences; 430074 Wuhan, China*

* Corresponding author: Zizheng Guo (cuggzz@cug.edu.cn)

Abstract: It's widely accepted that future environmental changes will affect rainfall-induced shallow slides in high-mountain areas. In this study, the Val d'Aran region located in the Central Pyrenees was selected to analyse and quantify the impacts of land use and land cover (LULC) and climate changes on regional landslides susceptibility. We analysed 26 climate models of the EURO-CORDEX database focussing on the future rainfall conditions. The IDRISI TerrSet software suite was used to create the future LULC maps. These two inputs were analysed individually and in a combined way defining 20 different scenarios. All these scenarios were incorporated in a physically-based stability model to compute landslides susceptibility maps. The results showed that both environmental conditions will considerably change in the future. The daily rainfall will increase between 14% and 26% assuming a return period of 100 years. This intensification of precipitation will produce an overall decrease of the stability condition in the study area. Regarding the LULC prediction, the forest area will significantly increase, while in particular grassland, but also shrubs decrease. As a consequence, the overall stability condition improves, because the root strength is higher in forest than in grassland and shrubs. When we analysed the combined impacts, the results showed that the positive effect of LULC changes is larger than the negative influence of rainfall changes. Hence, when combining the two aspects in the future scenarios, the stability condition in the study area will improve.

Keywords: Shallow slope failure; Future environmental changes; Susceptibility; Physically-based model; Pyrenees

1. Introduction

Rainfall-triggered landslides are an important hazard in mountainous regions. Recent studies concluded that land use and land cover (LULC) and climate changes will have an important effect on the frequency and magnitude of rainfall-induced landslides (Gariano and Guzzetti 2016; Persichillo et al. 2017; Bernardie et al. 2021). However, the assessment of the effects of LULC and climate changes on shallow slides is complex and uncertainties are still very large.

Land use and land cover is widely recognized an important influencing factor in slope stability modelling, mainly because plant roots have reinforcement effect on soils and characteristics of hydraulic processes in slopes vary with vegetation types (Schwarz et al. 2010; Liu et al. 2016; Moos et al. 2016). Therefore, the landslide occurrence and density usually exhibit a clear relationship with different vegetation types (e.g., Dymond et al. 2006; Rossi et al. 2010). Meanwhile, land use and land cover can change a lot when continuous and frequent activities in both social and environmental systems occur, such as urbanization process, climate changes and modifications of socioeconomic structures (Promper et al. 2014; Goetz et al. 2015; Meneses et al. 2019). There are many studies that confirm the relationship between LULC and the occurrence of slope failures. For example, a descriptive analysis of the historic LULC evolution in New Zealand (Glade 2003), where geomorphic responses related to anthropogenic land cover changes was investigated. Beguería (2006) and Shu et al. (2019) analysed the effect of LULC on landscape dynamics in the Pyrenees, and found that vegetation recovery could decrease the occurrence of shallow slides. Similar results have been also confirmed by Schmaltz et al. (2017), in which multi-temporal landslide inventories in Austria were established based on remote sensing data. In addition, case studies from Italy analysed the effect of agricultural practices and land management in inducing regional landslides (Persichillo et al. 2017; Gariano et al. 2018), by using heuristic approach and multivariate analysis, respectively. Finally, some investigations applied physical-based stability models to analyse the impacts of future LULC changes on the spatial and temporal probability of landslides in a watershed (Vanacker et al. 2003) or in small catchments (Van Beek and Van Asch 2004; Reichenbach et al. 2014) . Although their research methods varied, all these studies supported the idea that LULC changes could affect the predisposition of mountainous areas to shallow slides. Therefore, it is critical to timely and accurately obtain the dynamic information on land use and land cover, especially when dealing with the issue of slope failures.

The assessment of climate change is challenging the scientific community and becoming an important task for decision makers. Two possible consequences of climate change have been recognized (IPCC 2014): i) one is related to the rainfall, predicting more extreme events and rather

constant annual rainfall amount (depending on study area); and ii) the other one is related to air temperature and the global warming, which is an unequivocal issue. Under such backgrounds, the impacts of climate change on shallow slides involve multiple aspects (e.g., Crozier 2010; Gariano and Guzzetti 2016). Regarding the rainfall, the occurrences and frequency of extreme rainfalls may exceed thresholds in a given area and trigger shallow slide (e.g., Shou and Yang 2015). Regarding the temperature increase, manifolds consequences such as changes in the evapotranspiration, soil cracking and vegetation cover can be expected and will affect the landslide susceptibility (e.g., Bernardie et al. 2021). Analysis and assessment of the effect of climate change on regional mass movements have been conducted in different regions worldwide, such as British Columbia (Jakob and Lambert 2009), the European Alps (Stoffel and Huggel 2012; Stoffel et al. 2014) and the Caucasus (Huggel et al. 2012). The methods used in these studies are mostly statistical techniques and sometimes numerical models. Additionally, geomorphologic approaches investigating historic records have also been applied. For example, Coe and Michael (2004) used ninety years of historical landslide records in Seattle to assess annual exceedance probability of rainfall-triggered landslides. Borgatti and Soldati (2010) or Dietrich and Krautblatter (2017) studied the relationship between historical landslide inventories and climate conditions, and found the evidence for enhanced landslide activity controlled by climate change at regional scale. Some other researchers quantitatively predicted the future climate development and potential landslide risks. For instance, detailed climate prediction models and their impacts on rainfall-induced slides or debris flows were performed in Italy and France (Turkington et al. 2016; Ciervo et al. 2017; Gariano et al. 2017). Alvioli et al. (2018) and Salciarini et al. (2016) applied the physically-based model TRIGRS and global/regional climate models (GCM and RCM) in Central Italy. The findings in all these studies confirmed the assumption that changes in rainfall and temperature have a range of impacts on shallow slope failures in high-mountain areas, including their location, frequency and magnitude (Peres and Cancelliere 2018).

Only a few studies focused on the combined effect of LULC and climate changes on landsliding. (Grandjean et al. 2018) evaluated and compared influences of several cases on landslide activities and proposed adequate solutions, taking the Pyrenees as the study area. Bernardie et al. (2021) assessed the influences of these two changes on landslide hazard from the present to 2100 through the construction of various prospective socioeconomic and emissions scenarios and stated that both future changes will have significant impacts.

It is evident that attention of the scientific community to these topics is increasing, because the information on future landslide occurrence is fundamental for an adequate mitigation of the risk. Unfortunately, the specific evolution of the different governing factors and their effects are complex, and the uncertainties associated with the applied approaches and their parameters are still large (Coe

and Godt 2012).

Since only limited attempts have been made to predict the specific impacts of both LULC and climate changes on shallow slides at regional scale, the main aim of the present study is to assess and compare the influence of these two future changes on landslide susceptibility in the high mountain area of Val d'Aran located in the Central Pyrenees. The specific objectives include: i) the determination of future scenarios of LULC and climate in the study area, ii) the quantitative assessment of landslide susceptibility under different scenarios by applying a physically-based model, iii) the analysis and comparison of the impacts associated with both LULC and climate change.

2. The Val d'Aran study area

2.1. General Settings

The Val d'Aran region, which is situated in the Spanish part of the Central Pyrenees (Figure 1), was selected as study area because of two principal reasons. First, it represents a typical high mountain region that is affected by slope failures and that will undergo multiples changes in the future. Second, there is a detailed landslides inventory, which can be used for the calibration of the model parameters.

The study area covers 325.6 km^2 and is situated in the headwaters of the Garonne River (Figure 1). The altitude of the capital Vielha and the main valley floor is about 1000 m asl. , while the highest peaks reach almost 2750 m asl. The morphology is marked by fluvial, glacial and peri-glacial processes (e.g., Pallàs et al. 2006). The last glaciations during the Upper Pleistocene produced steep valley slopes and accumulated moraine sediments that cover the bedrock, while fluvial-torrential processes and gravitational mass movements formed the present landscape. From a geological point of view, the Val d'Aran is located in the Axial Pyrenees, where bedrock is principally constituted by Paleozoic rock, folded during the Hercinian orogeny, and intrusions of tardohercinian plutonic rocks (Fontboté 1991; Muñoz 1992).

The area is characterized by an Alpine Atlantic climate, which is influenced by the west winds from the Atlantic Ocean and the orographic effects of the Pyrenees. The mean annual temperature is between 5 and 9 °C, while the mean annual precipitation ranges from about 900 mm in the valley floor to 1200 mm on the highest peaks (GENCAT 2008).

The present land use and land cover in the study area principally includes forest (43.1 % of total area), grassland (30.8 %) and shrubs (16.7 %), while weathered bedrock (3.7 %) and scree deposits (4.3 %) have minor importance (MCSC-4; CREAF 2020). In contrast, intact bedrock, bare soil, water or urban zones covers neglecting surfaces with less than 1 % of the total study area. An interesting fact is related to the slope orientation: shrubs and grassland are more abundant on south-facing slopes,

while forested areas are more common on north-facing slopes (Shu et al. 2019).

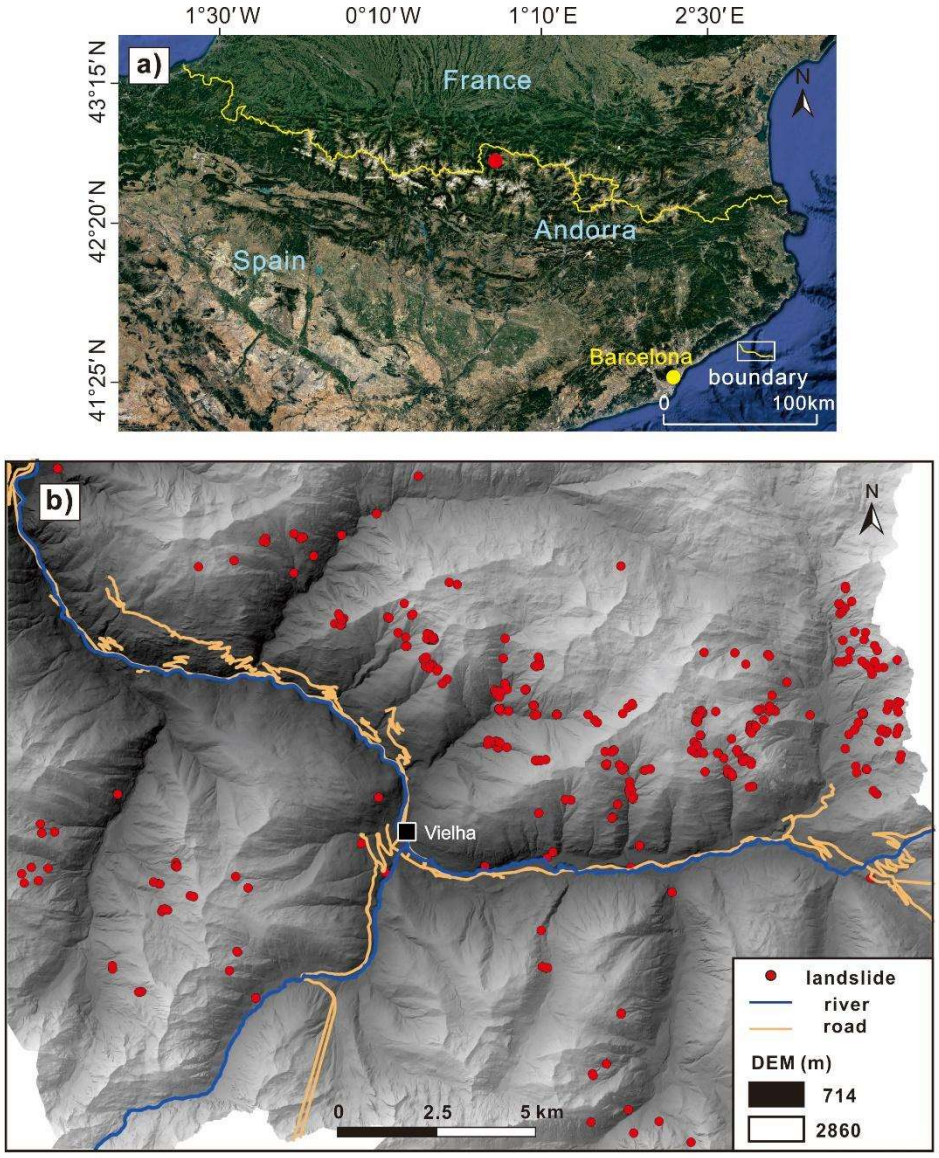

Figure 1: The Val d'Aran study area. a) Location of the study area in the Pyrenees (red dot). b) Digital Elevation Model (DEM) with shaded relief and the landslides triggered by the 2013 episode.

2.2. The 2013 landslide episode

On June 17th and 18th 2013, multiples landslides and important flooding occurred in the Val d'Aran region due to a combination of both heavy rainfall and snowmelt causing a total economic loss of more than 100 M€ (Oller et al. 2013; Victoriano et al. 2016; Shu et al. 2019). Rainfall of 124.7 mm in 48 h and 101.2 mm in 24 h were measured at the meteorological station of Vielha, while reports from the meteorological and water agencies indicate significant amount of snowmelt before and during the rainfall episode (CHE 2014).

After the landslide episode, a detailed inventory with 392 entries was created by interpretation of aerial photographs, helicopter flights and field surveys (Oller et al. 2013; Shu et al. 2019). The most common landslides were shallow slides and debris flows (channelized and open-slope ones). Most governing factors of the slope failures were assessed in Shu et al. (2019) and the results showed that landslides were more frequent at steep, south-facing slope with no vegetation or grass coverage. Herein, the lithology and LULC were re-analysed, because these two factors are directly related to soil properties incorporated in our physically-based stability model (see section 3.2 for details).

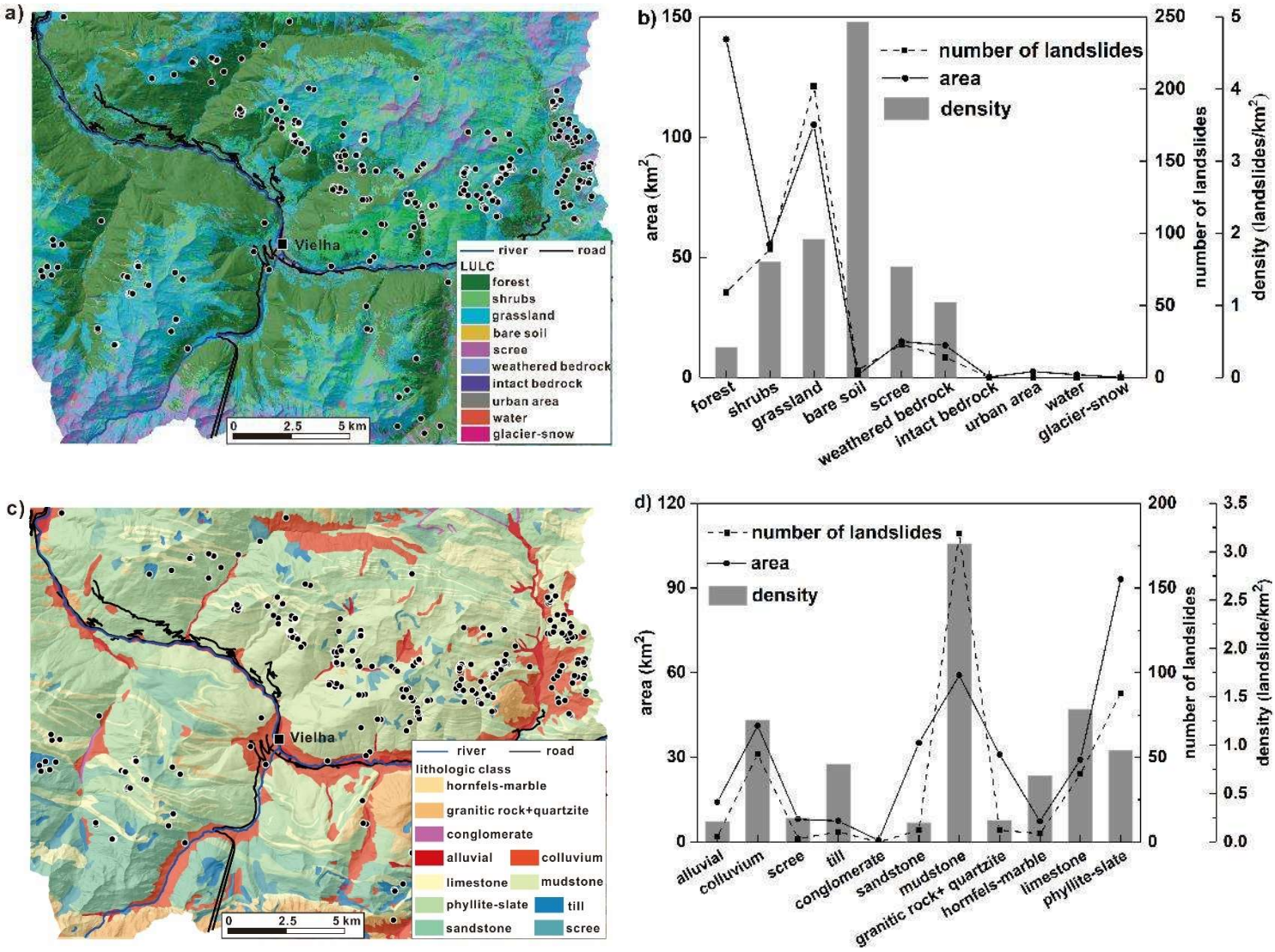

Figure 2: The effect of LULC and lithology on the landslide included in the inventory of the 2013 episode. a) Reclassified LULC map of 2009 and b) the influence of each class on the slope failure. c) Reclassified lithologic map and d) the influence of each class on the slope failure.

The effect of LULC on the 2013 slope failures was studied by reclassifying the LULC map of 2009 (CREAF, 2020). Finally, 10 categories were defined and the analysis of the inventory showed that most landslides occurred in grassland, while shrubs and forest are in second and third position (Figure 2b). In contrast, the most susceptible category, which is the one with the highest landslide density, corresponds to bare soil. As already detected in Shu et al. (2019), there is a clear influence of the vegetation on the landslide occurrence. This relation between vegetation and slope-failure probability is given by the positive trend between the density and vegetation. The ascending order of the landslide density is: forest, shrubs, grassland and finally bare soil.

The lithological influence was studied transforming the existing geological map (ICGC 2017) into 11 categories. Transformation from geological into lithological maps is complicate (Segoni et al. 2020) and related to uncertainty when used in physically-based landslide models (e.g., Tofani et al. 2017).The interpretation of the landslide density of the 2013 episode showed that areas with bedrock of mudstone were the most susceptible for slope failures during the 2013 episode, while areas of granite, quartzite, sandstone and conglomerate were much less susceptible (Figure 2).

3. Modelling strategy and parameter calibration

3.1. General overview

The overall modelling strategy includes three principal parts (Figure 3): i) the calibration of the parameters that are incorporated in the stability model using the landslide inventory of the 2013 episode, ii) the future predictions of land use and land cover (*LULC*) and climate changes, and iii) the calculation, assessment and comparison of future landslide susceptibility conditions using the stability model.

The first part focusses on the calibration of the parameters used in the stability model and includes two types of parameters. On one side, there are the parameters that can be kept constant over time, principally including the ones related to the geotechnical properties of the lithological classes. On the other side, there are the parameters that are affected by future vegetation or climate changes, which are variable over time. All the parameters were calibrated using the landslide episode that occurred in the Val d'Aran region in 2013. First, the runoff modelling was performed and the Curve Number (*CN*), for the different *LULC* categories was determined. Then, the stability modelling was carried out and the soil properties as well as the root strength (C_r) were fixed.

In the second part, the future predictions of climate and *LULC* changes were determined. It must be stated that regarding the climate changes, only rainfall was investigated, while *LULC* and rainfall changes were treated independently in the future predictions. The methodology applied during this

second part will be comprehensively explained in the next sections. In general, the climate and *LULC* conditions for three future time periods (herein called near, mid and far future) were predicted and compared with the present conditions (herein called reference scenario). While the output of the *LULC* prediction is directly a *LULC* map, the prediction of the future rainfall scenarios was carried out using the existing rainfall maps and a multiplier factor, M_i , determined for each of the three time period i (near, mid and far future; see section 4.1 for details). The rainfall was calculated for each of the three future time periods and the return periods of one (T_1), ten (T_{10}), and hundred (T_{100}) years.

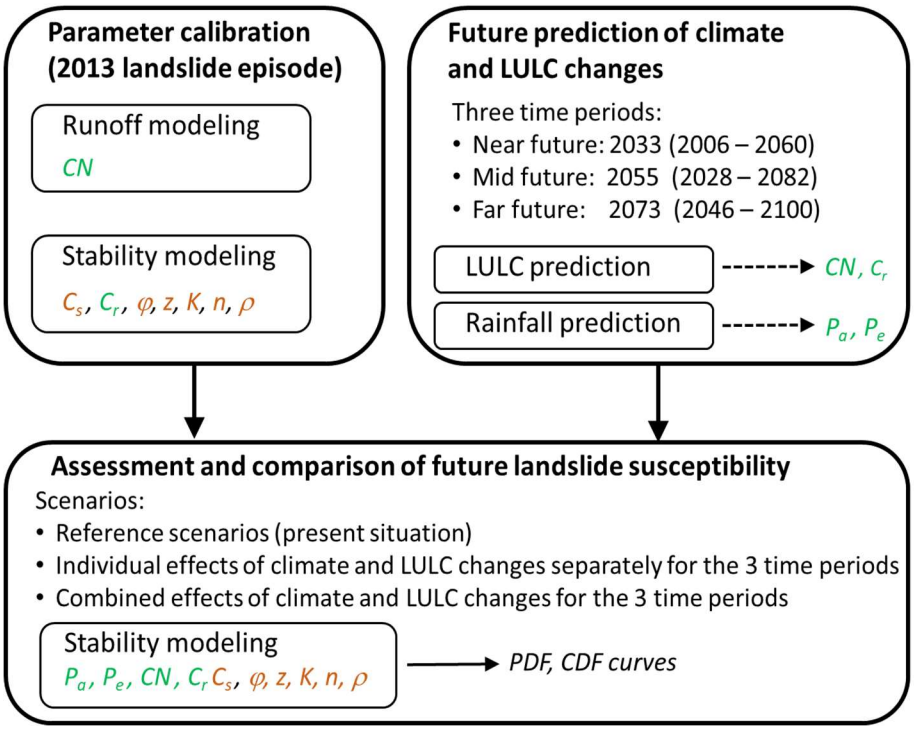

Figure 3: General overview of the modelling strategy applied in this study. Parameters marked in brown are static (related to soil properties) and parameters marked in green are variable (related to vegetation and climate changes) in the future scenarios. See text of the stability modelling section for parameter abbreviations.

Finally, the stability model was applied under different scenarios incorporating the outputs of the two previous steps (Figure 3). The landslide susceptibility was calculated in the entire study area for the three future time periods focussing first on the impacts of climate and LULC changes separately and then in a combined way. All the results were compared with the reference scenario, which is characterised by the most recent *LULC* map of 2009 (CREAF 2020) and the rainfall data obtained from the atlas elaborated for flood hazard assessment by the Spanish Ministry of Public Works and Transport (Santamaría and Parrilla 1999).

In total, ten different simulation runs were performed for each of the two selected return periods T_{10} and T_{100} of the triggering rainfall (P_e) (Table 1). The assessment of the triggering rainfalls with a 100-year return period is interesting when dealing with extreme events, while the results for T_{10} rainfall are necessary for comparison. In contrast, T_1 rainfall conditions were not included in the stability modelling, because only few landslides are expected to be triggered.

Table 1 Scenario definition considering *LULC* and climate changes. Climate changes only includes the variation of event rainfall (P_e). All the scenarios were calculated for the return periods T_{10} and T_{100}. P_{pres}-map indicates the present rainfall distribution in the study area. M_i is the multiplier factor for the climate prediction toward three time periods *i* (near, mid and far future).

Scenario	LULC (year)	Event rainfall, P_e
Reference scenario	2009	P_{pres}-map
Near future LULC	2033	P_{pres}-map
Mid future LULC	2055	
Far future LULC	2073	
Near future climate	2009	P_{pres}-map * M_{near}
Mid future climate	2009	P_{pres}-map * M_{mid}
Far future climate	2009	P_{pres}-map * M_{far}
Near future climate and LULC	2033	P_{pres}-map * M_{near}
Mid future climate and LULC	2055	P_{pres}-map * M_{mid}
Far future climate and LULC	2073	P_{pres}-map * M_{far}

3.2. Model description

The Fast Shallow Landslide Assessment Model (FSLAM) is a physically-based model developed for calculating landslide susceptibility at regional scale (Medina et al. 2021). In this study, an additional runoff model, which calculates the discharge in each cell of the study area, was integrated. Both models are described in continuation.

3.2.1. Stability modelling

The FSLAM model includes two different sub-models (Medina et al. 2021): i) the hydrological model, which calculated the rainfall infiltration into the soil layer and the resulting position of the water table, and ii) the geotechnical model, which applies the widely used infinite slope theory (Lambe

and Whitman 1979; Pack et al. 1998) to calculate the slope stability. The equation used to calculate the factor of safety (*FS*) can be expressed as:

$$FS = \frac{C_s + C_r}{g\rho_s z \cos\cos\theta \sin\sin\theta} + \left(1 - \left(\left(\frac{a}{b}\right)\frac{q_a}{Kz\sin\sin\theta \cos c \quad \theta} + \frac{q_e}{n \cdot z}\right)\left(\frac{\rho_w}{\rho_s}\right)\right)\left(\frac{\tan\tan\varphi}{\tan\tan\theta}\right) \quad (1)$$

where C_s is the effective cohesion of the soil matrix, C_r is the apparent cohesion produced by the root strength, g the gravity, ρ_s is the density of the saturated soil, z is the soil depth, θ is the terrain slope, a is the drainage area, b is the cell size, q_a is the effective infiltration rate due to antecedent rainfall, K is the horizontal hydraulic conductivity, q_e is the storm event infiltration, n is the soil porosity, ρ_w is the density of water, ϕ is internal friction angle.

The simplified hydrological model incorporates the effects of both the antecedent rainfall, which is applied by a lateral flow approach, and the storm event infiltration, which is included by a vertical flow approach. They can be calculated as follows:

$$q_a = P_a \quad (2)$$

$$q_e = P_e - \frac{\left(P_e - (\frac{5080}{CN} - 5\ )\right)^2}{P_e + 4 \cdot (\frac{5080}{CN} - 51)} \quad (3)$$

where P_a is the antecedent rainfall, P_e is the event rainfall, and *CN* is the curve number.

Among all the input parameters, six are static ones (Figure 3) and depend on the soil type, including C_s, φ, ρ_s, K, n, and z. Two parameters are dynamic or variable ones and depend on the vegetation, namely C_r and *CN*. In addition, two parameters are related to the rainfall (P_a and P_e) and therefore are also dynamic ones. Finally, all this information is included in five input raster files (Digital Elevation Model, *DEM*; soil properties; *LULC*; and the two rainfall files, P_a and P_e) and two text files.

To overcome the uncertainty of soil properties, a stochastic approach was proposed, where the parameters related friction angle and cohesion can be selected as stochastic values within a given range. Hence, the model allows to obtain the probability of failure (*PoF*), when the stochastic parameters are used.

3.2.2. Runoff modelling

The runoff module linked to FSLAM provides the water discharge in each raster cell of the study area during a rainfall event. The parameter, which determines the runoff and the infiltration in a simplified manner, is the *CN*. The so-called *CN* method has been widely used in hydrology (Yu, 1998; Woodward et al., 2002; Mishra and Singh, 2013), although its limitations (Ponce and Hawkins 1996). In our model strategy, we take advantage of the dual interpretation of *CN* (infiltration, runoff), because it is possible to easily adjust the infiltration and runoff during a rainfall event using the observed runoff

at selected points in the drainage network.

The discharge is computed using the rational method (Chow et al. 1988), which requires the tributary area, the rainfall intensity and the runoff coefficient. The tributary area is computed using a standard D8 cumflow algorithm (O'Callaghan and Mark 1984). The runoff coefficient (*C*) is computed using the following equation, which was adapted for Spanish catchments by (Témez 1991):

$$C = \frac{(P_e - I_a)\cdot(P_e + 23I_a)}{(P_e + 11I_a)^2} \quad (4)$$

Where *Pe* is the event rainfall and I_a is the initial abstraction computed from the *CN*. Finally, the rainfall intensity *I* is computed using the Spanish Intensity-Duration-Frequency (*IDF*) curves (Témez 1978):

$$I = I_d 11^{\left(\frac{28^{0.1} - T_C^{0.1}}{28^{0.1} - 1}\right)} \quad (5)$$

where I_d is the daily rainfall intensity, and T_c the concentration time, which is defined as

$$T_c = 0.3\left(\frac{L}{j^{0.25}}\right)^{0.76} \quad (6)$$

where *L* is the longest distance from the watershed divide to the outlet, and *j* is the average slope.

3.3.Calibration of parameters

As explained in the general overview of the modelling strategy, the 2013 episode was selected to calibrate the multiple model parameters (Figure 3). This calibration phase included two steps: first, the runoff modelling focusses on the curve number *CN*; and, second, the stability modelling calibrates the soil properties C_s, ϕ, *z*, *K*, *n*, ρ and the root cohesion C_r.

3.3.1. Input data

The stability and runoff modelling needed five input raster files (*DEM*; soil properties; *LULC*; P_a and P_e). The *DEM* was obtained from ICGC (2013) and has a 5 m resolution. The soil as well as the LULC maps were reclassified from the official cartography and included 11 (soil) and 10 (LULC) categories, respectively (Figure 2). The two rainfall inputs were determined by using the available data on precipitation and snowmelt (Pineda et al. 2013; CHE 2014). The area affected by snowmelt was determined by satellites images, while the quantity was estimated by snow-height measurements at the weather stations. The final distribution of the effective water recharge into the terrain previous to the landslide episode (P_a raster) included two different values: 0.5 mm/d for the areas with no snowmelt and 1.0 mm/d for the areas, where snowmelt can be assumed to have added extra water into the soil (Figure 4a). The data of the water input for P_e was estimated combining the rainfall observed at the different weather stations and the snowmelt that occurred during the landslide episode (Figure 4b).

The snowmelt related to P_e was approximated by 60 mm, which represent approximately 20 cm of snow assuming a snow density of 30%.

All the five raster files were prepared at a 5 m cell size, which gives a total amount of 13 million of pixels for the entire study area. FSLAM is a code focused on efficiency and simplicity, and therefore, computational time for one run was only about 3 minutes using a computer with one 8-cores 1.8 GHz *CPU* and 8 GB of *RAM*. This short computational time was very helpful, or even necessary, during the iterative calibration procedure.

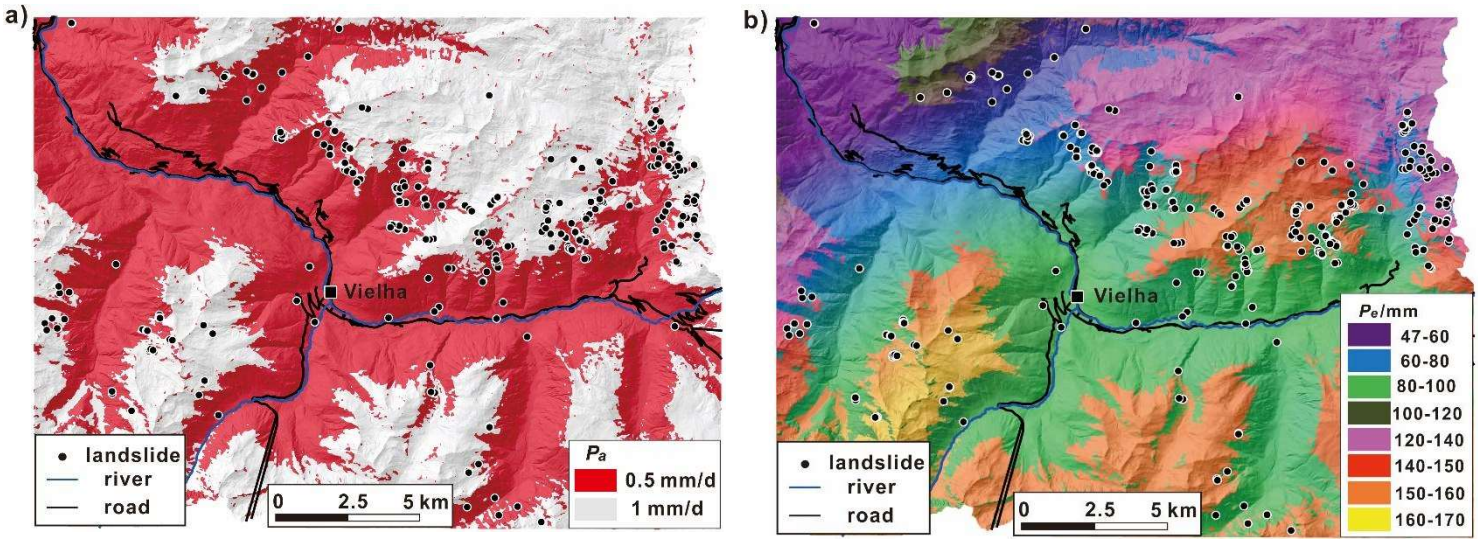

Figure 4: Rainfall and snowmelt conditions of the 2013 landslide episode used for the model calibration. a) Antecedent water recharge, P_a, and b) event water recharge, P_e. Both maps include the locations of the landslides that were used during the calibration phase.

3.3.2. Runoff modelling

The runoff modelling focussed on the calibration of the curve number. The *CN* values were initially selected according to the ranges proposed by the Catalan Water Agency and the USDA (USDA 1986; Montalbán et al. 2013) and subsequently refined by an iterative approach fitting the discharge observed at two gauge stations. The gauge stations are located in the higher part of the Garone River basin (Arties) and at the outlet of our study area (Bossost, Figure 5). Both stations were severely damaged during the flood episode, but peak discharges were estimated as 170 m^3/s for Arties and 300 m^3/s for Bossost (CHE 2014). The simulated runoff at these points were 144.4 m^3/s (Arties) and 336.3 m^3/s (Bossost), respectively. Therefore, compared with the observed values, the errors for both stations were less than 15%, which was acceptable for such a simplified approach and the existing uncertainties.

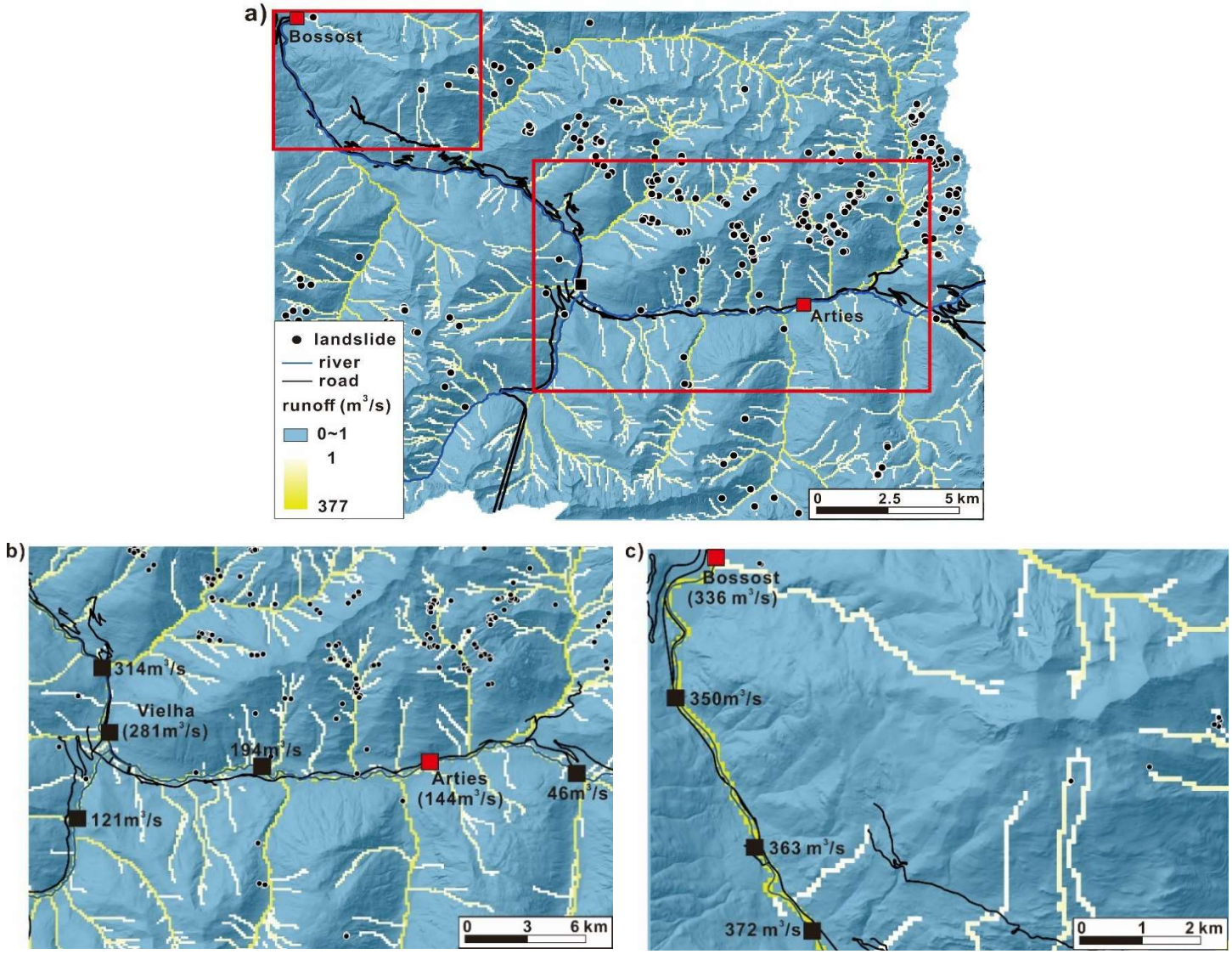

Figure 5: Runoff calculated for the 2013 episode and calibration of *CN*.

3.3.3. Stability modelling

In this step, the static parameters were calibrated, which included the soil parameters (C_s, φ, h, K, n, ρ) and the root cohesion (C_r). The values were determined by an iterative approach applying receiver operating characteristic (*ROC*) techniques and focussed on the accuracy of the outcome. The best-fit parameter values coincide well with published data and are shown in Table 2 and Table 3. In addition, the resulting landslide susceptibility map adopting these values is shown in Figure 6.

Table 2 Best-fit values of the soil properties obtained during the calibration phase. The properties are separated regarding the different lithological classes. *HSG* stands for hydrologic soil group (USDA 2007)

Lithological class	C_s - min/max (kPa)	φ- min/max (º)	h (m)	K (m/s)	n (-)	ρ (kg/m^3)	*HSG* (-)
alluvial	0/3	35/45	4	1×10^{-3}	0.3	2000	A
colluvium	1/3	25/35	1.5	1×10^{-6}	0.3	2000	B
scree	0/3	40/50	3	1×10^{-2}	0.4	2000	A
till	0/5	30/40	2	1×10^{-5}	0.3	2000	B
conglomerate	0/5	35/45	3	1×10^{-5}	0.35	2000	A
sandstone	1/5	35/45	3	1×10^{-4}	0.35	2000	A
mudstone	1/5	20/30	2	1×10^{-6}	0.3	2000	B
granitic rock+ quartzite	0/4	35/45	2	1×10^{-5}	0.3	2000	A
hornfels-marble	1/3	30/40	2	1×10^{-5}	0.3	2000	A
limestone	1/3	20/35	1.5	1×10^{-6}	0.3	2000	B
phyllite-slate	0/5	20/35	2	1×10^{-6}	0.3	2000	B

Table 3 Best-fit values of the root cohesion (C_r), and the curve number (*CN*), obtained during the calibration phase. The values are separated regarding the different LULC classes.

LULC	C_r -min/max (kPa)	*CN-A* (-)	*CN-B* (-)	*CN-C* (-)	*CN-D* (-)
forest	4/14	40	60	69	76
shrubs	3/6	43	65	76	82
grassland	2/4	49	69	79	84
bare soil	0/0	77	86	91	94
scree	0/0	30	30	30	30
weathered bedrock	0/0	77	86	91	94
intact bedrock	0/0	77	86	91	94
urban area	0/1	90	92	96	98
water	999/999	100	100	100	100
glacier-snow	999/999	100	100	100	100

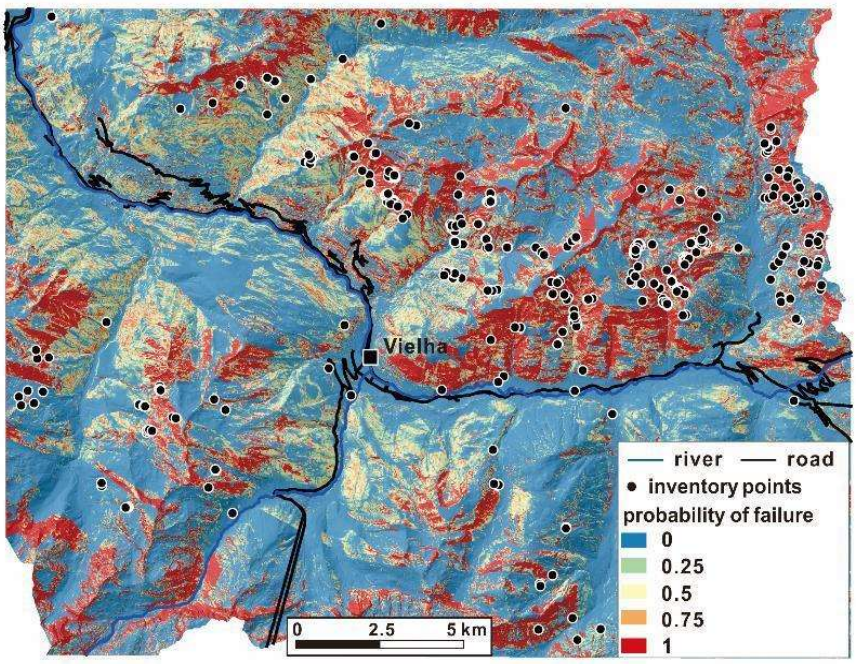

Figure 6: Probability of failure map obtained from the stability modelling of the 2013 landslide episode using the best-fit values of the soil properties, root strength and curve number.

To evaluate the accuracy of our simulations, 5000 points were randomly selected in the study area and their *PoF* values were compared with the 392 landslide inventory points. The percentage of points versus the *PoF* (Figure 7a) showed the important destabilizing effect of the 2013 rainfall episode. While most selected points had a *PoF* less than 0.2 prior to the episode (no rainfall inputs), approximately 60% of the inventory points changed to *PoF* larger than 0.9, when the rainfall and snowmelt of the 2013 was incorporated. On the contrary, such a change was not observed for the dataset of random points. In the random dataset, both scenarios had the largest number of points in a *PoF* range of 0 and 0.1. A more specific view of these results is shown in a 3D plot (Figure 7b). It can be seen that most random and inventory points had *PoF* values less than 0.125 previous to the incorporation of the snowmelt and rainfall into the stability calculations (PoF_{pre}). In contrast, the *PoF* values of most inventory points ranged between 0.875 and 1.0 posterior of the incorporation of the effects of the 2013 episode (PoF_{post}).

In addition, fuzzy logic curves showing the effect of the 2013 episode on the *PoF* evolution were plotted (Figure 7c). The curves show that the number of inventory points gradually increases with higher *PoF* values, while the random points showed the opposite trend. All these results lead us to conclude that the increase of *PoF* for the inventory points during the 2013 episode was evident, while it was very small for the random points. An additional proof of a correct calibration of our model was

the value of the area under the curve ($AUC = 0.78$), which was determined by the *ROC* curve (Figure 7d). Hence, the performance of the present stability model was satisfactory unless the multiple uncertainties and the parameters obtained from this calibration phase can be used for the future prediction.

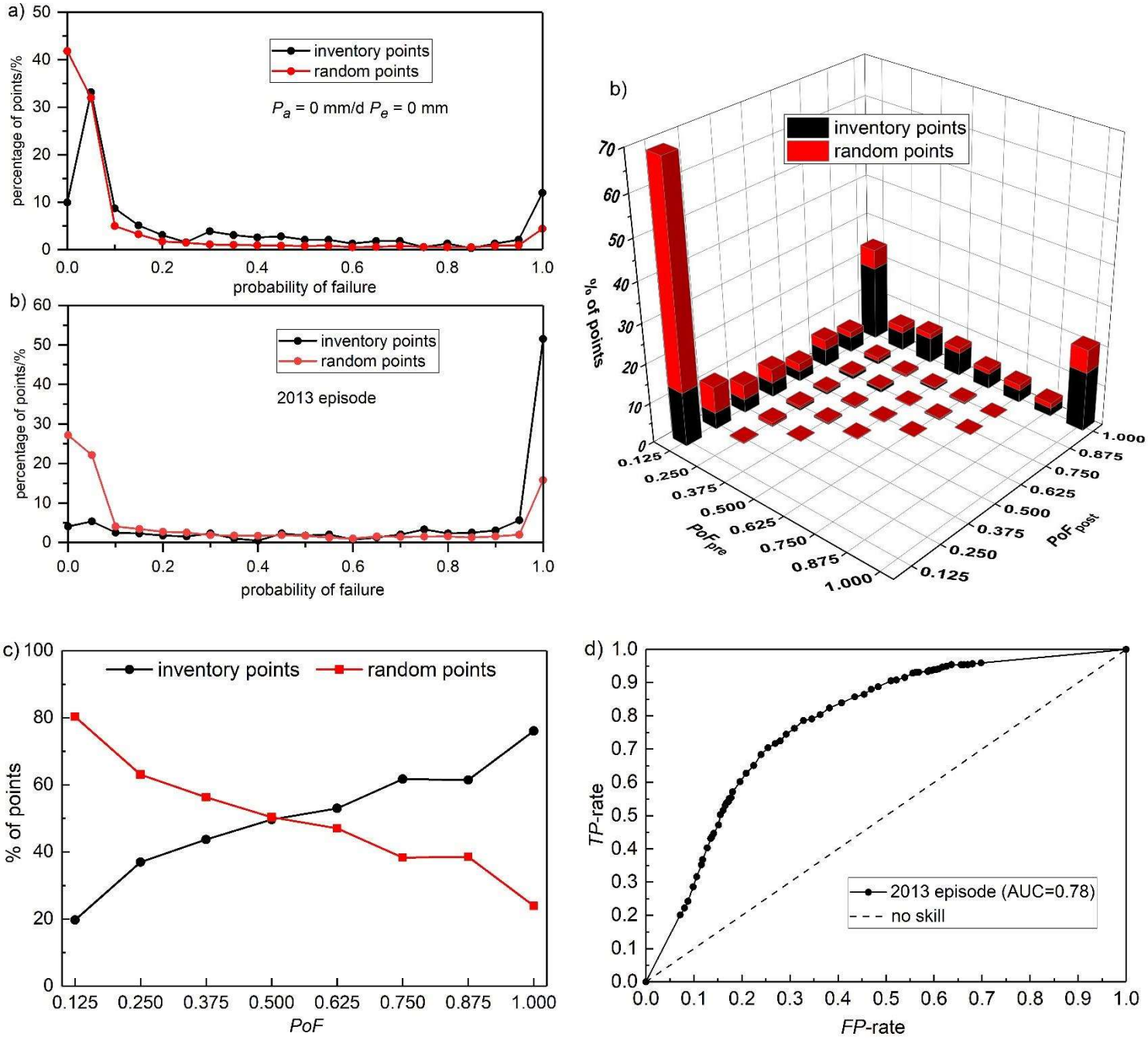

Figure 7: Evaluation of the stability modelling for the 2013 landslide episode. Comparison of the inventory with randomly selected points using probability of failure (*PoF*), and 2D- (a) and 3D-plot (b). c) Fuzzy logic curves representing the effect of the 2013 episode. d) False Positive (*FP*) rate versus True Positive (*TP*) rate of *ROC* curve and *AUC* value.

4. Impacts of future climate changes

4.1. Prediction of future rainfall patterns

Global Climate Models (GCMs) are able to reproduce the characteristics of recent and past climate, and predict how the climate will be in the future applying physical principles and climate scenarios. Atmosphere-Ocean General Circulation Models provide quantitative estimates of climate change on a global scale with a good level of confidence for some essential climate variables, for example temperature, but with substantial uncertainties for other variables such as precipitation (e.g., Flato et al., 2013). The Regional Climate Models (RCMs), which are needed for practical applications, are capable of reproducing the most important climatic characteristics at regional scale with high resolution, but the existence of significant biases is known (Kotlarski et al., 2014). While some of these deficiencies are specific to some models, other drawbacks appear to be a common and systematic feature inherited from GCMs used as boundary conditions.

The dynamical downscaling experiment CORDEX, a successor of ENSEMBLES, provides regional climate results, facing the experiments proposed by the Coupled Model Intercomparison Project Phase 5 (CMIP5). In the present work, we have selected the six RCMs from the EURO-CORDEX project (Jacob et al. 2014), which are driven by the five GCMs (

Table 4). Therefore, we analysed a total of 26 climate models with a spatial resolution of approximately 12 km under the future Representative Concentration Pathways (RCP) 8.5, in order to study climatic extreme events in a worst-case scenario. After a short initial phase comparing the data of different pixels in the Val d'Aran region, we focussed on the daily rainfall time-series of the pixel located in the centre of the main valley. The 1951 to 2005 period was selected as the historical reference time window for almost all climate models. The model data were divided in three time periods of 55 years with partial overlapping, as described in the previous section: 2006 - 2060 (near future), 2028 - 2082 (mid future) and 2046 - 2100 (far future).

Table 4 Relation of the 26 climate models used in this work and their relation to the corresponding RCM and GCM.

RCM / GCM	CCLM4-8-17 (CLMcom)	RCA4 (SMHI)	RACMO22E (KNMI)	HIRHAM5 (DMI)	WRF (IPSL)	REMO15 (GERICS)	REMO09 (MPI)
MPI-ESM-LR	RCM01	RCM02	RCM03	RCM04	RCM06		RCM08
IPSL-CM5A-MR		RCM12	RCM13		RCM16	RCM17	x
HadGEM2-ES-MOHC	RCM21	RCM22	RCM23	RCM24	RCM26		
EC-EARTH ICHEC	RCM31	RCM32	RCM33	RCM34	RCM36		
CNRM-CM5	RCM41	RCM42	RCM43	RCM44	RCM46	RCM47	

The stability model FSLAM includes two rainfall inputs: the antecedent rainfall and the event or triggering rainfall. In a preliminary step, the prediction of the antecedent rainfall was studied by analysing the annual rainfall time-series. The results showed that the annual precipitation is rather constant and no significant increase or decrease was detected. This general outcome is supported by other studies carried out in the Pyrenees and the North-eastern part of the Iberian Peninsula (e.g., Castro et al., 2005; OPCC-CTP, 2018; MedECC, 2020). Therefore, we focussed in this study on the event rainfall, which was analysed as described in the following.

An initial check of the daily precipitation time series provided by the 26 RCMs showed that the bias, uncertainties and differences are too high to allow a reliable and consistent analysis. To overcome this difficulty the analysis is performed by comparing the historical and the projected time series for each RCM.

First, we analysed the rainfall associated with frequencies less than or equal to three occurrences per year. The frequencies of precipitation ranges in the historical and future time series were compared, using 5 mm intervals. The rainfall events that are repeated an average of three times annually would be the equivalent to the 95th percentile for days with precipitation (Acero et al. 2011). The comparison was carried out dividing the RCM projections into the three time periods (near, mid and far future), which contain the same number of years as the historical series (55 years).

The comparison is used to calculate a future climate trend for frequencies. These trend values were calculated for the 26 RCMs, the three time periods and the return periods of 2, 5, 10, 25, 100 and 500 years. Thus, a total 468 trend values were computed. Due to the large variability in the 26 RCMs, the 90th percentile was determined for each of the three time periods and the six return periods. The 90th percentile of the trend values was used in the subsequent steps, in order to define a worst scenario

assumption but avoiding outliers. The 78 trend values and the 90th percentiles corresponding to the three time periods are plotted in Figure 8 for the example of the rainfall return period of 100 years. The meaning of the trend is that values larger than unity suggest that extreme rainfall events will occur more frequently in the future. The figure perfectly reflects the large variability of the climate models.

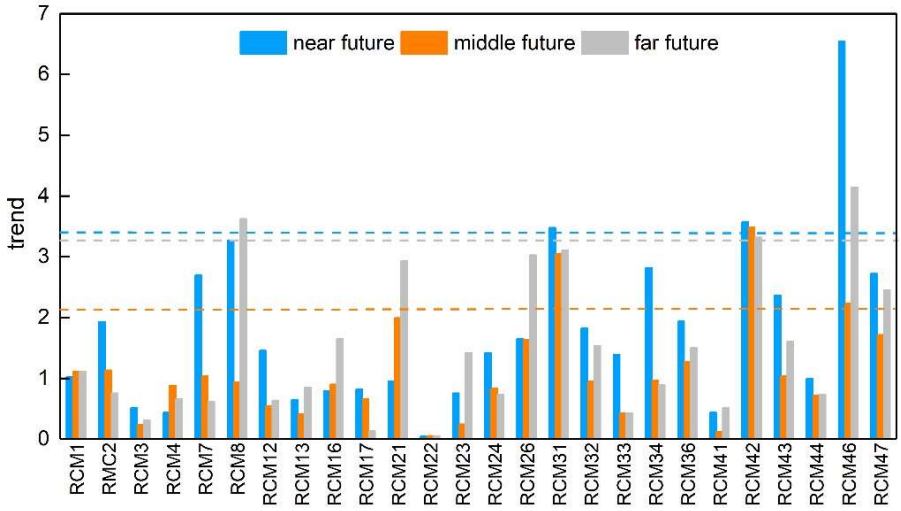

Figure 8: Prediction of future rainfall patterns. Example of trend values calculated for the 26 RCMs and the three future time periods showing results related to the return period of 100 years. The horizontal dashed lines indicate the 90th percentiles for each of the three time periods. Trend values larger than unity suggest that extreme rainfall events will occur more frequently in the future.

The proposed methodology permits us to calculate a trend for the future frequency evolution of extremes. In the next step, the actual return period precipitations are assigned to their future frequency obtaining a shifted precipitation-frequency plot. The ratio between the actual and the future precipitations for the different return periods is defined as multiplier factor. This frequency-based method avoids using directly the precipitation values and just relies on the frequency evolution.

The multiplier factor (M_i) was determined for each of the three time periods i (near, mid and far future) and the two return periods T_{10} and T_{100}. The obtained M_i values show that the increase of the event rainfall in the future is between 14 and 26% and that maximums are observed in the near and far future (Table 5). These results confirm the outcomes of other studies that propose an augment of extreme rainfall events in general and in particular in mountainous regions (e.g., IEC, 2017; OPCC-CTP, 2018).

Finally, the multiplier factor was applied to the current precipitation maps of the study area, which are published by the Spanish Ministry of Public Works and Transport (Santamaría and Parrilla 1999), in order to determine a spatially distributed map of the event rainfall, later used as an input for the stability simulations.

Table 5 Multiplier factor obtained for the three time periods and two rainfall return periods.

	near future (2006 - 2060)	mid future (2028-2082)	far future (2046-2100)
T_{10}	1.23	1.14	1.22
T_{100}	1.26	1.16	1.25

4.2. Landslide susceptibility under future rainfall changes

The susceptibility maps of the future rainfall scenarios were calculated with the raster file of the event rainfall as described above. In contrast, the antecedent rainfall, which corresponds to a representative water recharge into the soil, was defined by a constant value of 0.6 mm/d over the entire study area. This value was estimated from the actual annual precipitation published by the Spanish Ministry of Public Works and Transport and was defined as invariable input in the future scenarios. In addition, the LULC input raster file was the one of the reference scenario (year 2009). Finally, six different scenarios were simulated using *FSLAM* (Table 5).

The example of the landslide susceptibility map obtained from the stability modelling for T_{100} and the far future time period is shown in Figure 9. Since the event rainfall will increase in the future, the overall stability decreases. To better visualize the future trend, the *PoF* map of the future scenario was subtracted with map of the reference scenario and *PoF* differences were calculated in each cell of the entire study area. These maps of *PoF* differences show that most zones will suffer slightly worse stability conditions in the future and there is a generalized *PoF* increase of a few percentages in the study area.

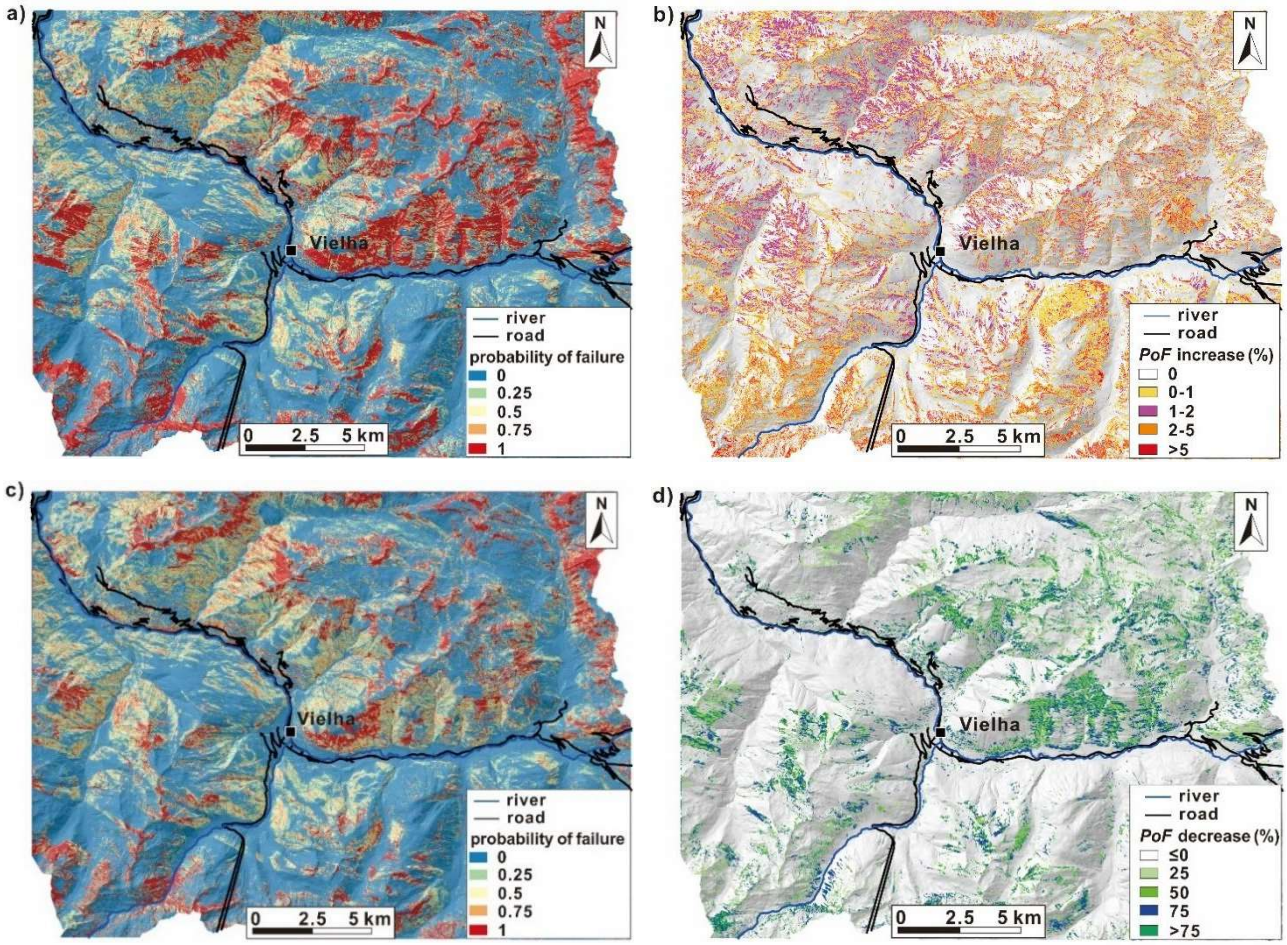

Figure 9: Landslide susceptibility maps indicating the climate (upper row) and *LULC* (lower row) impacts for the far future time period. a) *PoF* map for rainfall scenario of the time period 2046 – 2100 and the 100-years rainfall return period. b) *PoF* difference map between the future and the reference (year 2009) scenario. c) *PoF* map for the *LULC* scenario of 2073. d) *PoF* difference map between the future and reference scenario.

For a better interpretation of the results, the cumulative distribution function (*CDF*) and the probability density function (*PDF*) of each resulting map was calculated, and the *CDF* as well *PDF* curves were plotted for the corresponding *PoF* values. Then, the area under the *CDF* curve (AUC_{CDF}) was computed in order to summarize the overall stability condition in the study area by one single value (Table 6). In addition, the *normalized PDF* was determined by dividing the *PDF* of the future scenario with the one of the reference scenario.

The results of the climate change impacts for the reference as well as the three future scenarios

are shown in Figure 10a and b regarding the T_{100} rainfall conditions. The different curves confirm that the increase of event rainfall in the future only slightly reduces the overall stability conditions in the study area. While this trend is difficult to appreciate in the *CDF* curves, the *normalized PDF* curves better reveal this small drift to more instable conditions. N*ormalized PDF* values larger than 1.0 for unstable conditions (high *PoF* values) support this drift, while *normalized PDF* values around 1.0 (*PoF* up to 0.3) indicate that there is no change in stability. Although there is this slight and overall reduction of stability, the *CDF* curves reveal that half of the study area (*CDF* equal to 0.5) is characterized by totally stable conditions (*PoF* less than 0.1).

The small reduction of the overall stability in the study area was not only obtained for the T_{100} rainfall conditions, but also for the return period of T_{10}. The AUC_{CDF} values of all the simulated scenarios confirm this outcome (Table 6). Especially, the differences of the AUC_{CDF}, which were calculated by comparing the reference and future scenario, reveal that the global reduction of stability is small. In addition, there is only a small difference of the overall stability in the study area comparing the three different time periods. The simulations for near and far future scenarios have a slightly lower overall stability conditions than the mid future scenario.

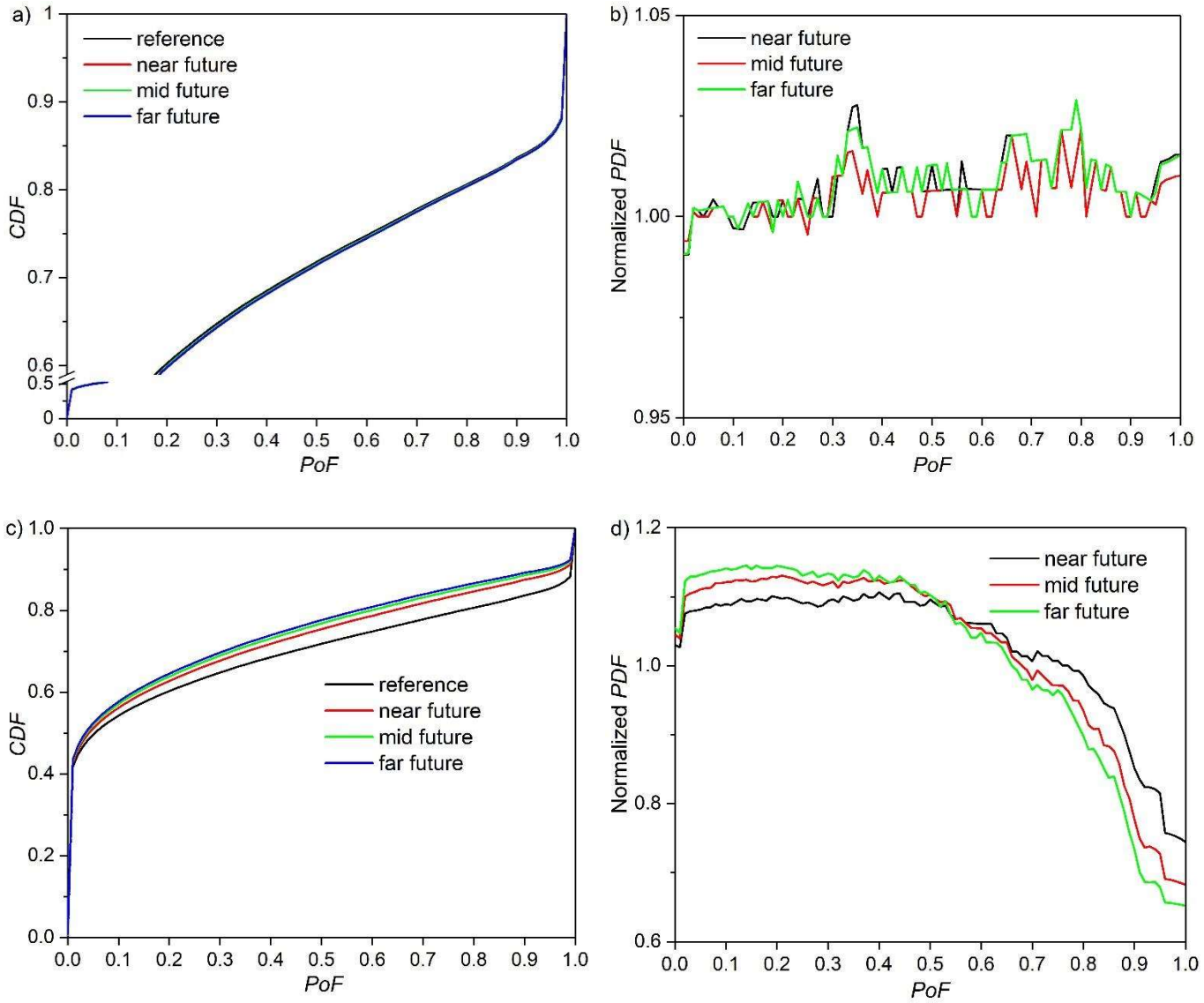

Figure 10: Impacts of the future rainfall (upper row) and LULC (lower row) changes. The cumulative distribution function (*CDF*) versus probability of failure (*PoF)* for the reference as well as the three future time period scenarios are plotted in the left column (a and c). The normalized probability distribution function (*PDF*) versus *PoF* are plotted in the right column (b and d). The impacts of the 100-years rainfall return period is shown.

Table 6 Values of the area under the *CDF*-curve (AUC_{CDF}) for all the analysed scenarios and the two return periods T_{10} and T_{100}. In addition, the difference between the reference and future scenario is given as ΔAUC_{CDF} .

	T_{10}		T_{100}	
	AUC_{CDF}	ΔAUC_{CDF}	AUC_{CDF}	ΔAUC_{CDF}
Reference scenario	0.707	-	0.701	-
Near future LULC changes	0.739	+0.032	0.733	+0.032
Mid future LULC changes	0.751	+0.044	0.744	+0.042
Far future LULC changes	0.758	+0.051	0.751	+0.050
Near future climate changes	0.704	-0.003	0.697	-0.004
Mid future climate changes	0.705	-0.002	0.699	-0.002
Far future climate changes	0.704	-0.003	0.697	-0.004
Near future climate and LULC changes	0.736	+0.029	0.729	+0.028
Mid future climate and LULC changes	0.749	+0.042	0.742	+0.041
Far future climate and LULC changes	0.755	+0.048	0.748	+0.047

5. Impacts of future LULC changes

5.1. Methods and data

The IDRISI TerrSet software was used to perform LULC prediction (Eastman 2015). This software package includes a module called Land Change Modeler (LCM) that allows users to analyse the future LULC changes. The reclassified LULC maps of 1993 and 2009 were used as main input (CREAF 2020). In addition, seven predictor variables were determined as the substantial drivers of LULC changes. These variables were determined according to previous studies (Molowny-Horas et al. 2015; Shu et al. 2019) and can be divided into three categories:

i) Topographical variables: The digital elevation model with a 5 m resolution was used to generate slope and aspect maps using the “raster terrain analysis” tool in QGIS.

ii) Climatic variables: The annual precipitation and average temperature between 1961 and 1990 were downloaded from the Climatic Atlas of Catalonia (GENCAT 2008). This means that future climate changes were not included in the LULC modelling, because this aspect was analysed separately as described in the previous sections.

iii) Landscape variables: The distributions of urban area and rivers can affect the LULC changes.

Hence, the distances to roads and river networks was calculated at each pixel. Given that the construction and expansion of infrastructures in this mountainous area are slower than the change rates of other LULC types, both variables were set as static variables.

Before the modelling process, we transformed all the input files into the same reference system, the same resolution (5 m) and the same spatial extension. Then, the LCM analysed the transition between the different LULC classes using the maps of 1993 and 2009. Subsequently, the set of predictor variables was used as the drivers of LULC changes to fit every transition during this period. After the training process, the transition potential was created, which is used to analyse the future LULC changes and generates the LULC map of a given year (Eastman 2015). In our case, we calculated the maps for the following three years: 2033 for the near future, 2055 for the mid future and 2073 for the far future scenario (Figure 3).

5.2. Prediction of future LULC scenarios

The historic and future evolution of the LULC classes in the study area is shown in Figure 11a. For the historical period between 1993 and 2009, the LULC evolution revealed considerable changes. The forest and shrubs increased by 16.5% and 5.4%, respectively, while the grassland decreased by 20%. This may be associated with the fact that the shrubs and forest ecosystems extended as a result of the decrease in the rural population and abandonment of pasture during the last century (Roura-Pascual et al. 2005; Beguería 2006). Except these three LULC classes, the change of the other classes was not important and their total areas were much smaller.

Regarding the future LULC prediction, the results show that historic trends are mostly continuing in the future. The most evident change is related to the increase of forest area and the decrease of grassland (Figure 11). During the entire simulation period from 2009 to 2100, the total area of the forest largely increased by 45.2%, while the grassland decreased by 43.2%. Their changes are not linear, but gradually decreases over time. In particular the area of grassland diminishes by 29 km^2 during 2009 - 2050, while only by 14.3 km^2 between 2050 and 2100. This means that the average decreasing rate is about the double during the first period. In addition, the scree area slightly increases by 5.2%. The bare soil, weathered bedrock and urban areas decrease by 0.18 km^2, 3.69 km^2, and 0.79 km^2, respectively. On a whole, the predictive results fit rather well with the ones obtained by previous studies (e.g., Shu et al. 2019).

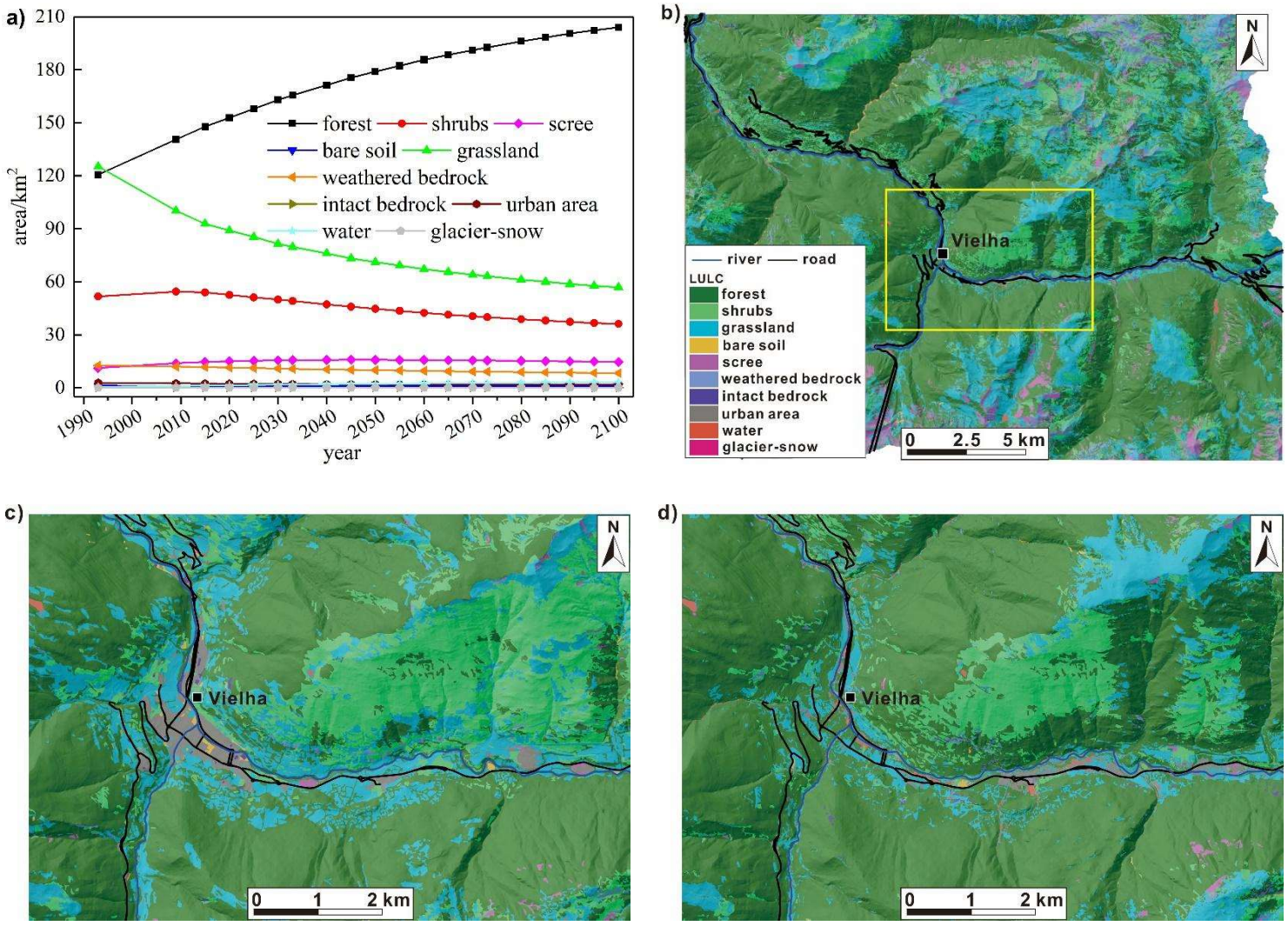

Figure 11: Results of the LULC prediction. a) Historic and future evolution of the LULC classes in the study area. b) The LULC prediction for the far future time period (year 2073). The yellow rectangle indicates the area shown in c) and d). c) Zoomed area of the reference scenario (year 2009), d) Zoomed area of the LULC prediction for the far future (year 2073).

5.3. Landslide susceptibility under future LULC changes

The three maps with the LULC-predictions for 2033, 2055 and 2073 were used as the input raster files for the stability calculations, while the rainfall inputs were taken from the reference scenarios. The resulting landslide susceptibility maps clearly show an overall increase of stability. As examples, we present the results related to far future scenarios and the T_{100} rainfall return period (Figure 9c and d). Regarding the area of low landslide susceptibility ($PoF < 0.25$), the percentage of this area in the reference scenario with a T_{100} rainfall return period was 62.6%, and it rose to 65.3% (near future),

66.5% (mid future), and 67.2% (far future), respectively in the future scenarios. In contrast, the percentage of the area with high landslide susceptibility ($PoF > 0.75$) decreased from 20.8% (reference scenario) to 16.8% (near future), 15.5% (mid future), and 14.7% (far future), respectively. Similar results were obtained for the T_{10} rainfall return period.

The improved stability conditions in the future are mainly associate with the increased forest areas and the corresponding higher cohesion values because of the higher root strength in forest. This confirms the positive impact of tree roots on stabilizing the slope, which has been published in multiples studies (e.g. Lan et al. 2020).

The impacts of the *LULC* changes were also analysed by the *CDF* and *normalized PDF* curves, which were calculated for the different scenarios. The curves that represent the T_{100} rainfall are shown in Figure 10 and allow us to better visualize the changes of landslide susceptibility in the future. By comparing the future scenarios with the result obtained from the reference scenario, the increase of stability can perfectly be observed. Regarding the *CDF* curves, it's clearly visible that the *CDF* value is increasing in the future for almost the entire *PoF* range. The stabilizing trend for the future scenarios is even more evident when looking to the *normalized PDF* curves (Figure 10d). There is a considerable increase of the *normalized PDF* value for stable conditions (small *PoF* values) and a large decrease for instable conditions (high *PoF* values).

This overall improvement of stability in the study area was also obtained for the scenarios with a T_{10} rainfall condition and is supported by the AUC_{CDF} values (Table 6). Summarising the results related to future *LULC* changes, all the ΔAUC_{CDF} values increased between 0.032 and 0.051, which reflect a trend towards an overall more stable situation in the future for our study area.

6. Comparison and evaluation of the impacts of future changes

Finally, the individual as well as the combined effect of *LULC* and climate changes were compared. As stated in the modelling strategy, the *LULC* and climate changes were incorporated in the stability calculations as independent factors. Therefore, the combined simulations for the different scenarios were performed with the two corresponding *LULC* and P_e input raster files (Table 1), and there are no interactions between our future predictions of land cover and rainfall.

The *CDF*, *PDF* and normalized *PDF* curves as well as the AUC_{CDF} and the ΔAUC_{CDF} values of all the individual and combined scenarios were compared. The *CDF* and normalized *PDF* curves for the combined scenario and the T_{100} rainfall return period is plotted in Figure 12 and shows that the overall stability in the study area will increase in the future. This can be explained with the fact that the positive effect of LULC (especially the increase of forest area and the associated higher root

cohesion) is much larger than the negative influence of larger event rainfalls. The values of AUC_{CDF} and ΔAUC_{CDF} clearly visualise this trend, since the ΔAUC_{CDF} values for the LULC impact is between +0.032 and +0.051, while the same values for the effect of future rainfall changes are between -0.002 and -0.004 (Table 6).

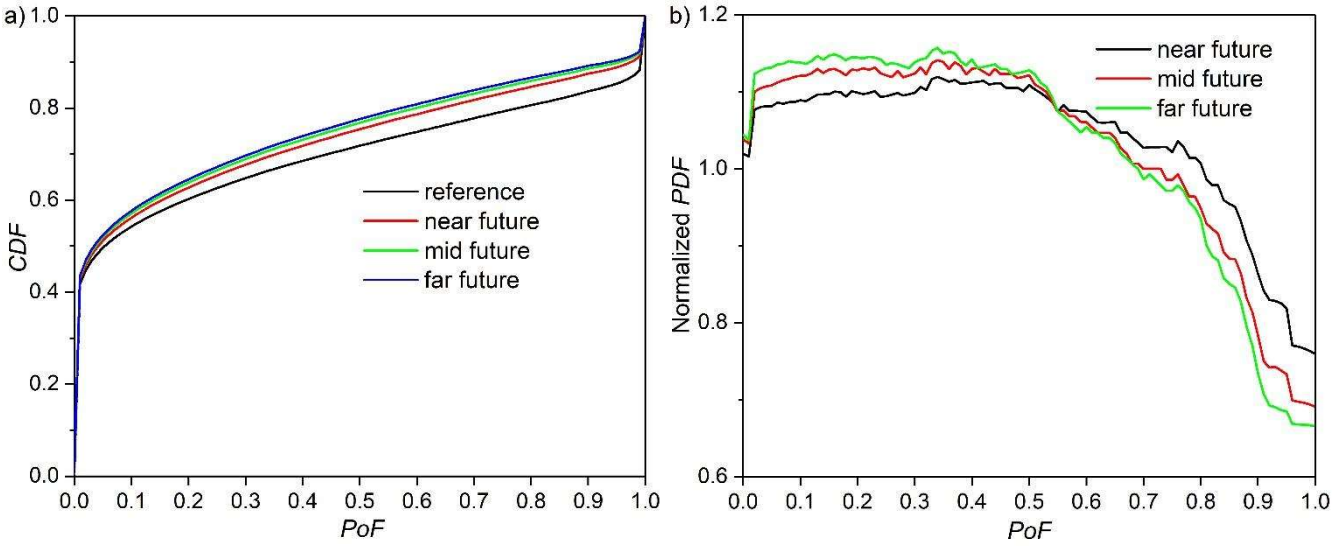

Figure 12: Impacts of combined rainfall and LULC changes for the reference as well as the three future time period scenarios and the 100-years rainfall return period. a) Cumulative distribution function (*CDF*) versus probability of failure (*PoF*) in the study area, b) normalized probability distribution function (*PDF*) versus *PoF*.

In order to evaluate the impacts of all the future scenarios by a final and summarising graph, the normalised *CDF* values were calculated for three different *PoF* values by subtracting the *CDF* values of the future scenarios with the one of the reference scenario (Figure 13). The three *PoF* values 0.5, 0.8, and 0.9 were selected to conduct this analysis. The results confirm the previous outcomes that the stabilizing influence of the *LULC* changes is considerably larger than the destabilizing effects related to rainfall changes. Therefore, when the combined impacts of the two changes were considered, the normalized *CDF* values increase, which confirms that the overall stability in the study area will improve. The results also show that the overall stability increase with time and the most stable conditions are predicted for the far future time period.

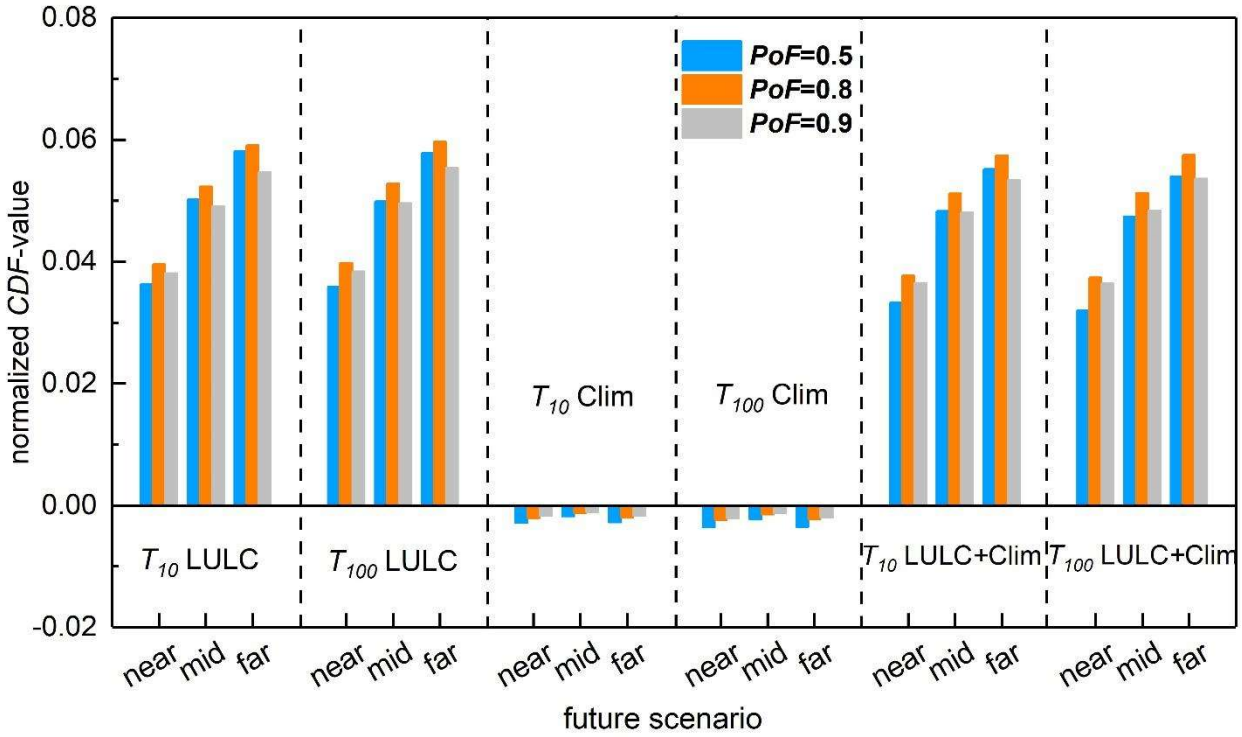

Figure 13: Comparison of all scenarios calculated in this study using the normalized *CDF* values for three different *PoF* values. *LULC* stands for land use and land cover and *Clim* for climate change scenarios, while T_{10} and T_{100} represent the rainfall return periods.

7. Discussion

Two major topics are discussed in the following. First, the uncertainties that are associated with the specific outcomes will be debated, and second, our results will be compared with the ones of other studies.

The uncertainties regarding the stability model and future changes are mainly related to one of the following aspects: i) the values or value ranges of the soil properties and the root cohesion; ii) the LULC prediction and the resulting changes of the root strength, and, iii) the rainfall prediction that defines the future event rainfall. Regarding the first aspect, there are six input parameters in the FSLAM model that depend on the lithological category. In the infinite slope approach, the cohesion is the most important parameter for the model results, followed by the internal friction angle (Medina et al. 2021). Therefore, these two parameters are included as stochastic parameters. However, the stochastic approach, which is incorporated in our model only incorporates the uncertainty on values of these two parameters not their spatial distribution. The spatial distribution of the different soil types was determined from the regional geological map, which is a very difficult task (Tofani et al. 2017;

Segoni et al. 2020). Hence, a technique that considers the spatial uncertainties may be of high interest. In fact, some methods on this topic have been proposed (e.g., Salciarini et al. 2017; Lizárraga and Buscarnera 2019), but they are rather time-consuming and not applicable for stability assessment over very large areas. Finally, our calibration results showed that the uncertainty in the input parameters for the modelling are acceptable. The error of the runoff modelling ranged from 12% to 15%, and the stability model accuracy expressed by the *ROC* curve was 78%.

The uncertainty related to the second aspect, the LULC predictions, has multiples origins, among which state the predictive variables. A well-known viewpoint is that although topographic conditions and initial vegetation are important to understand the vegetation dynamics, the socioeconomic factors play another, crucial role (Roura-Pascual et al. 2005). Hence, to better predict the future LULC scenarios, users may select reasonable environment and society variables as the inputs. They are considered as the drivers of the land cover transformation and can directly influence the predictive results. However, it is difficult to quantify the factors associated with the socioeconomic development over large mountainous areas. In our prediction model, the distance to road and distance to rivers were selected as a proxy, but they only can coarsely reflect the distribution of urban areas and population in the region.

It should also be noted that the LULC prediction is influenced by other environmental factors like the effect of wildfires in forest areas (Nyman et al. 2011; Rengers et al. 2020). This effect should certainly be in future investigations. In the Val d'Aran region, however, the main LULC changes have generally been explained as a result of agriculture land abandonment during the 20th century (Beguería 2006; García-Ruiz et al. 2010). Indeed, this trend is also rather common in many other mountainous areas in Europe (MacDonald et al. 2000). Therefore, a similar stabilizing trend may be expected in other areas. This assumption is supported by other studies focussing on the positive effect of forest on landsliding (e.g., Schmaltz et al. 2017).

The uncertainties regarding the prediction of future rainfall conditions are dominantly associated with the inter-model variability, whereas inter-scenario and internal model variability is of secondary importance (Giorgi and Francisco 2000). Our outcomes support this point, since the results obtained from the 26 RCMs are very heterogeneous. In fact, other studies from the Pyrenees concluded that precipitation errors may exceed 10% (López-Moreno et al. 2013; OPCC-CTP 2018). Therefore the 90th percentile, which was selected in our study as the value for the future predictions, seems to be reasonable. However, our results show that the impacts of a 90th percentile rainfall change is less important than the expected *LULC* change.

In addition, it is necessary to mention that in this study the multiples variables related to climate changes were reduced to the daily rainfall time series, which is a strong simplification. The increase

of temperature associated with the global warming may be another important factor that influence slope stability (Gariano and Guzzetti 2016) and there are other factor indirectly related to landslide activity like evapotranspiration, soil cracking etc. (Crozier 2010). All these factors may change the final results but were considered out of scope in this study focussing on general trends at regional scale.

The final outcome of our study revealed that the impacts on susceptibility of *LULC* changes is much larger than the one related to rainfall changes. A direct comparison of our results with the ones of other studies described in literature is difficult, since only very few investigations have included both aspects. Bernardie et al. (2021) analysed the effects of *LULC* and climate changes in a basin of the French Pyrenees and concluded that the landslide occurrence is expected to increase in the future. However, their study area was much smaller (70 km^2) then ours and large parts were already covered by forest. Therefore, the increase of forested area in the future was very small, which may explain the smaller effect of *LULC* changes. Scheidl et al. (2020) analysed the landslide susceptibility in two headwater catchments of the Eastern Alps and focussed especially on the forest development. Although their objectives were different from ours, the main conclusions coincide, since they propose that climate change may increase landslide activity, but root cohesion plays an important role for stabilization. Other studies that only include one of the two future changes support our outcomes regarding climate changes (e.g., Gariano et al. 2017), while the impacts of vegetation changes may be more dependent on local characteristics (e.g., Reichenbach et al. 2014).

8. Conclusions

Future environmental changes are assumed to affect shallow slope failures in high-mountain areas. In the present study, the impacts of future land cover and rainfall changes on regional-scale shallow slides were assessed applying a physically-based model and 20 different scenarios. The analysis revealed the following three main outcomes:

- The daily rainfall will increase between 14% and 26 % assuming a rainfall return period of 100 years. The higher daily rainfall would produce lower overall stability conditions regarding the entire study area.
- The LULC predictions showed that the forest area will significantly increase, while in particular grassland, but also shrubs will decrease. These changes would create better overall stability conditions due to higher root strength in the areas that evolve into forest.
- When the effects of both changes were compared, an important finding was that the stabilizing effects of LULC changes are larger than the destabilizing ones of rainfall changes. Hence, when the two impacts are assessed in the future scenarios, the overall stability conditions in the study

area will improve.

Many assumptions and simplifications were introduced and uncertainties exist, but the general trend towards better stability conditions is very clear in the Val d'Aran region. Even using the high-emissions RCP8.5 global warming scenario and the 90th percentile of the rainfall trends, the effect of rainfall changes is less important than the one related to the future expected *LULC* changes. Our conclusions may be applied to other high-mountain areas with similar environmental characteristics since agriculture land abandonment is not a site-specific trend.

In spite of the uncertainties and the necessity of additional research, the outcomes of the present study can be an important help for administrations and stakeholders to determine appropriate land-use planning. Relevant measures such as extensive afforestation and avoiding deforestation will be useful policies for reducing the hazard associated with rainfall-triggered shallow slides in the future.

Acknowledgements

This study was funded by the national research project EROSLOP (PID2019-104266RB-I00/AEI/10.13039/501100011033) of the Spain Government. Zizheng Guo acknowledges the financial support of China Scholarship Council for his research at UPC BarcelonaTECH, and Fundamental Research Funds for National Universities, China University of Geosciences (Wuhan).

References

Acero FJ, García JA, Gallego MC (2011) Peaks-over-threshold study of trends in extreme rainfall over the Iberian Peninsula. J Clim 24:1089–1105. https://doi.org/10.1175/2010JCLI3627.1

Alvioli M, Melillo M, Guzzetti F, et al (2018) Implications of climate change on landslide hazard in Central Italy. Sci Total Environ 630:1528–1543. https://doi.org/https://doi.org/10.1016/j.scitotenv.2018.02.315

Beguería S (2006) Changes in land cover and shallow landslide activity: A case study in the Spanish Pyrenees. Geomorphology 74:196–206. https://doi.org/10.1016/j.geomorph.2005.07.018

Bernardie S, Vandromme R, Thiery Y, et al (2021) Modelling landslide hazards under global changes: The case of a Pyrenean valley. Nat Hazards Earth Syst Sci 21:147–169. https://doi.org/10.5194/nhess-21-147-2021

Borgatti L, Soldati M (2010) Landslides as a geomorphological proxy for climate change: A record from the Dolomites (northern Italy). Geomorphology 120:56–64.

https://doi.org/10.1016/j.geomorph.2009.09.015

Castro M, Martin-Vide J, Alonso S (2005) The climate of Spain: past, present and scenarios for the 21st century. A Preliminary General Assessment of the Impacts in Spain Due to the Effects of Climate Change. Ministerio de Medio Ambiente, 62pp.

CHE (2014) Informe de la avenida del 17 al 20 de junio de 2013 en la cuenca del río Garona. Confederación Hidrográfica del Ebro. Ministry for the Ecological Transition (In Spanish)

Chow VT, Maidment DR, Mays LW (1988) Applied Hydrology. International Edition, McGraw-Hill Book Company, New York

Ciervo F, Rianna G, Mercogliano P, Papa MN (2017) Effects of climate change on shallow landslides in a small coastal catchment in southern Italy. Landslides 14:1043–1055. https://doi.org/10.1007/s10346-016-0743-1

Coe J, Michael J (2004) Probabilistic assessment of precipitation-triggered landslides using historical records of landslide occurrence, Seattle, Washington. Environ Eng Geosci 10:103–122. https://doi.org/10.2113/10.2.103

Coe JA, Godt J (2012) Review of approaches for assessing the impact of climate change on landslide hazards. In: Eberhardt E, Froese C, Turner AK, Leroueil S (eds) Landslides and Engineered Slopes. Banff, Canada, pp 371–377

CREAF (2020) The Land Cover Map of Catalonia. https://www.creaf.uab.es/mcsc/ Accessed 22 October 2020

Crozier MJJ (2010) Deciphering the effect of climate change on landslide activity: A review. Geomorphology 124:260–267. https://doi.org/10.1016/j.geomorph.2010.04.009

Dietrich A, Krautblatter M (2017) Evidence for enhanced debris-flow activity in the Northern Calcareous Alps since the 1980s (Plansee, Austria). Geomorphology 287:144–158. https://doi.org/https://doi.org/10.1016/j.geomorph.2016.01.013

Dymond JR, Ausseil AG, Shepherd JD, Buettner L (2006) Validation of a region-wide model of landslide susceptibility in the Manawatu-Wanganui region of New Zealand. Geomorphology 74:70–79. https://doi.org/10.1016/j.geomorph.2005.08.005

Eastman JR (2015) TerrSet: Geospatial Monitoring and Modeling Software. Clark Las 53

Flato G, Marotzke J, Abiodun B, et al (2013) Evaluation of Climate Models. In: Stocker, TF; Qin, D; Plattner, GK; Tignor, M; Allen, SK; Boschung, J; Nauels, A; Xia, Y; Bex, V; Midgley P (ed) Climate Change 2013: The Physical Science Basis. Contribution of Working Group I to the Fifth Assessment Report of the Intergovernmental Panel on Climate Change. Cambridge University Press, Cambridge, UK and New York, NY, USA.

Fontboté J. (1991) Reflexions sobre la tectònica dels Pirineus. Memorias la Real Acad Ciencias y

Artes Barcelona Tercera ép:307-352.(In Spanish)

García-Ruiz JM, Beguería S, Alatorre LC, Puigdefábregas J (2010) Land cover changes and shallow landsliding in the flysch sector of the Spanish Pyrenees. Geomorphology 124:250–259. https://doi.org/10.1016/j.geomorph.2010.03.036

Gariano SL, Guzzetti F (2016) Landslides in a changing climate. Earth-Science Rev 162:227–252. https://doi.org/10.1016/j.earscirev.2016.08.011

Gariano SL, Petrucci O, Rianna G, et al (2018) Impacts of past and future land changes on landslides in southern Italy. Reg Environ Chang 18:437–449. https://doi.org/10.1007/s10113-017-1210-9

Gariano SL, Rianna G, Petrucci O, Guzzetti F (2017) Assessing future changes in the occurrence of rainfall-induced landslides at a regional scale. Sci Total Environ 596–597:417–426. https://doi.org/https://doi.org/10.1016/j.scitotenv.2017.03.103

GENCAT (2008) Climatic Atlas of Catalonia. https://territori.gencat.cat/ca/01_departament/12_cartografia_i_toponimia/bases_cartografiques/medi_ambient_i_sostenibilitat/atles-climatic/ Accessed 22 October 2020

Giorgi F, Francisco R (2000) Evaluating uncertainties in the prediction of regional climate change. Geophys Res Lett 27:1295–1298. https://doi.org/10.1029/1999GL011016

Glade T (2003) Landslide occurrence as a response to land use change: a review of evidence from New Zealand. CATENA 51:297–314. https://doi.org/https://doi.org/10.1016/S0341-8162(02)00170-4

Goetz JN, Guthrie RH, Brenning A (2015) Forest harvesting is associated with increased landslide activity during an extreme rainstorm on Vancouver Island, Canada. Nat Hazards Earth Syst Sci 15:1311–1330. https://doi.org/10.5194/nhess-15-1311-2015

Grandjean G, Thomas L, Bernardie S, et al (2018) A Novel multi-risk assessment web-tool for evaluating future impacts of global change in Mountainous Areas. Climate 6:. https://doi.org/10.3390/cli6040092

Huggel C, Clague JJ, Korup O (2012) Is climate change responsible for changing landslide activity in high mountains? Earth Surf Process Landforms 37:77–91. https://doi.org/10.1002/esp.2223

ICGC (2017) Geological map 1:50000. https://icgc.cat/en/Public-Administration-and-Enterprises/Downloads/Geological-and-geothematic-cartography/Geological-cartography/Geological-map-1-50-000. Accessed 22 Oct 2020

ICGC (2013) Terrain Elevation Model of Catalonia 5 x 5 meters. http://www.icc.cat/appdownloads/ Accessed 22 October 2020

IEC (2017) Third Report on Climate Change in Catalonia. Institute of Catalan Studies, Barcelona, 98 pp

IPCC (2014) Climate Change 2014: Synthesis Report Contribution of Working Groups I, II and III to the Fifth Assessment Report of the Intergovernmental Panel on Climate Change. R.Pachauri, L. Meyer (editors). Gevena, Switzerland, 151 pp.

Jacob D, Petersen J, Eggert B, et al (2014) EURO-CORDEX: New high-resolution climate change projections for European impact research. Reg Environ Chang 14:563–578. https://doi.org/10.1007/s10113-013-0499-2

Jakob M, Lambert S (2009) Climate change effects on landslides along the southwest coast of British Columbia. Geomorphology 107:275–284. https://doi.org/10.1016/j.geomorph.2008.12.009

Kotlarski S, Keuler K, Christensen OB, et al (2014) Regional climate modeling on European scales: A joint standard evaluation of the EURO-CORDEX RCM ensemble. Geosci Model Dev 7:1297–1333. https://doi.org/10.5194/gmd-7-1297-2014

Lambe TW, Whitman R V (1979) Soil mechanics. Wiley, New York

Lan H, Wang D, He S, et al (2020) Experimental study on the effects of tree planting on slope stability. Landslides 17:1021–1035. https://doi.org/10.1007/s10346-020-01348-z

Liu HW, Feng S, Ng CWW (2016) Analytical analysis of hydraulic effect of vegetation on shallow slope stability with different root architectures. Comput Geotech 80:115–120. https://doi.org/https://doi.org/10.1016/j.compgeo.2016.06.006

Lizárraga JJ, Buscarnera G (2019) Spatially distributed modeling of rainfall-induced landslides in shallow layered slopes. Landslides 16:253–263. https://doi.org/10.1007/s10346-018-1088-8

López-Moreno JI, Zabalza J, Vicente-Serrano SM, et al (2013) Impact of climate and land use change on water availability and reservoir management: Scenarios in the Upper Aragón River, Spanish Pyrenees. Sci Total Environ 493:1222–1231. https://doi.org/10.1016/j.scitotenv.2013.09.031

MacDonald D, Crabtree JR, Wiesinger G, et al (2000) Agricultural abandonment in mountain areas of Europe: Environmental consequences and policy response. J Environ Manage 59:47–69. https://doi.org/10.1006/jema.1999.0335

MedECC (2020) Summary for Policymakers. In: Climate and Environmental Change in the Mediterranean Basin – Current Situation and Risks for the Future. First Mediterranean Assessment Report [Cramer W, Guiot J, Marini K (eds.)] Union for the Mediterranean, Plan Bleu, UNEP. Marseille, France, 34pp

Medina V, Hürlimann M, Guo Z, et al (2021) Fast physically-based model for rainfall-induced landslide susceptibility assessment at regional scale. CATENA 201:105213. https://doi.org/10.1016/j.catena.2021.105213

Meneses BM, Pereira S, Reis E (2019) Effects of different land use and land cover data on the

landslide susceptibility zonation of road networks. Nat Hazards Earth Syst Sci 19:471–487. https://doi.org/10.5194/nhess-19-471-2019

Mishra S, Singh V (2013) Soil Conservation Service Curve Number (SCS-CN) Methodology (Vol.42), Springer Science & Business Media.

Molowny-Horas R, Basnou C, Pino J (2015) A multivariate fractional regression approach to modeling land use and cover dynamics in a Mediterranean landscape. Comput Environ Urban Syst 54:47–55. https://doi.org/10.1016/j.compenvurbsys.2015.06.001

Montalbán F, Manzano A, Correa L, et al (2013) Recomanacions tècniques per alsestudis d inundabilitat d àmbit local. Barcelona, Catalan Water Agency. (In Spanish)

Moos C, Bebi P, Graf F, et al (2016) How does forest structure affect root reinforcement and susceptibility to shallow landslides? Earth Surf Process Landforms 41:951–960. https://doi.org/10.1002/esp.3887

Muñoz JA (1992) Evolution of a continental collision belt: ECORS-Pyrenees crustal balanced cross-section. In: McClay KR (ed) Thrust Tectonics. Springer Netherlands, Dordrecht, pp 235–246

Nyman P, Sheridan GJ, Smith HG, Lane PNJ (2011) Evidence of debris flow occurrence after wildfire in upland catchments of south-east Australia. Geomorphology 125:383–401. https://doi.org/10.1016/j.geomorph.2010.10.016

O'Callaghan JF, Mark DM (1984) The extraction of drainage networks from digital elevation data. Comput Vision, Graph Image Process 28:323–344. https://doi.org/10.1016/S0734-189X(84)80011-0

Oller P, Pinyol J, González M, et al (2013) Efectes geomorfològics de l'aiguat i riuada del 18 de Juny de 2013. In: Gestió de les inundacions. pp 126-132.(In Spanish)

OPCC-CTP (2018) Climate change in the Pyrenees: Impacts, vulnerabilities and adaptation. Bases of knowledge for the future climate change adaptation strategy in the Pyrenees, 150 pp. ISBN:978-84-09-06268-3

Pack RT, Tarboton DG, Goodwin CN (1998) The SINMAP approach to terrain stability mapping. Eighth Int Congr Int Assoc Eng Geol Environ Proceedings, Vols 1-5 1157–1165

Pallàs R, Rodés A, Braucher R, et al (2006) Late Pleistocene and Holocene glaciation in the Pyrenees: a critical review and new evidence from 10Be exposure ages, south-central Pyrenees. Quat Sci Rev 25:2937–2963. https://doi.org/10.1016/j.quascirev.2006.04.004

Peres DJ, Cancelliere A (2018) Modeling impacts of climate change on return period of landslide triggering. J Hydrol 567:420–434. https://doi.org/10.1016/j.jhydrol.2018.10.036

Persichillo MG, Bordoni M, Meisina C (2017) The role of land use changes in the distribution of shallow landslides. Sci Total Environ 574:924–937.

https://doi.org/https://doi.org/10.1016/j.scitotenv.2016.09.125

Pineda N, Prohom M, Serra A, et al (2013) Causes que van provocar la riuada a la Val d'Aran el 18 de juny de 2013, in: Jornada Gestión de las inundaciones. Barcelona, Spain, 27–28 November 2013, 120–125. (In Spanish)

Ponce VM, Hawkins RH (1996) Runoff Curve Number: Has It Reached Maturity? J Hydrol Eng 1:11–19. https://doi.org/10.1061/(asce)1084-0699(1996)1:1(11)

Promper C, Puissant A, Malet JP, Glade T (2014) Analysis of land cover changes in the past and the future as contribution to landslide risk scenarios. Appl Geogr 53:11–19. https://doi.org/10.1016/j.apgeog.2014.05.020

Reichenbach P, Busca C, Mondini AC, Rossi M (2014) The Influence of Land Use Change on Landslide Susceptibility Zonation: The Briga Catchment Test Site (Messina, Italy). Environ Manage 54:1372–1384. https://doi.org/10.1007/s00267-014-0357-0

Rengers FK, McGuire LA, Oakley NS, et al (2020) Landslides after wildfire: initiation, magnitude, and mobility. Landslides 17:2631–2641. https://doi.org/10.1007/s10346-020-01506-3

Rossi M, Guzzetti F, Reichenbach P, et al (2010) Optimal landslide susceptibility zonation based on multiple forecasts. Geomorphology 114:129–142. https://doi.org/10.1016/j.geomorph.2009.06.020

Roura-Pascual N, Pons P, Etienne M, Lambert B (2005) Transformation of a rural landscape in the Eastern Pyrenees between 1953 and 2000. Mt Res Dev 25:252–261. https://doi.org/10.1659/0276-4741(2005)025[0252:TOARLI]2.0.CO;2

Salciarini D, Fanelli G, Tamagnini C (2017) A probabilistic model for rainfall—induced shallow landslide prediction at the regional scale. Landslides 14:1731–1746. https://doi.org/10.1007/s10346-017-0812-0

Salciarini D, Volpe E, Kelley SA, et al (2016) Modeling the Effects Induced by the Expected Climatic Trends on Landslide Activity at Large Scale. Procedia Eng 158:541–545. https://doi.org/10.1016/j.proeng.2016.08.486

Santamaría J, Parrilla A (1999) "Máximas lluvias diarias en la España Peninsular." Serie Monografías. Dirección General de Carreteras y Centro de Estudios y Experimentación de Obras Públicas Ministerio de Fomento: Madrid, Spain. (In Spanish)

Scheidl C, Heiser M, Kamper S, et al (2020) The influence of climate change and canopy disturbances on landslide susceptibility in headwater catchments. Sci Total Environ 742:140588. https://doi.org/10.1016/j.scitotenv.2020.140588

Schmaltz EM, Steger S, Glade T (2017) The influence of forest cover on landslide occurrence explored with spatio-temporal information. Geomorphology 290:250–264.

https://doi.org/https://doi.org/10.1016/j.geomorph.2017.04.024

Schwarz M, Preti F, Giadrossich F, et al (2010) Quantifying the role of vegetation in slope stability: a case study in Tuscany (Italy). Ecol Eng 36:285–291. https://doi.org/10.1016/j.ecoleng.2009.06.014

Segoni S, Pappafico G, Luti T, Catani F (2020) Landslide susceptibility assessment in complex geological settings: sensitivity to geological information and insights on its parameterization. Landslides 17:2443–2453. https://doi.org/10.1007/s10346-019-01340-2

Shou KJ, Yang CM (2015) Predictive analysis of landslide susceptibility under climate change conditions - A study on the Chingshui River Watershed of Taiwan. Eng Geol 192:46–62. https://doi.org/10.1016/j.enggeo.2015.03.012

Shu H, Hürlimann M, Molowny-Horas R, et al (2019) Relation between land cover and landslide susceptibility in Val d'Aran, Pyrenees (Spain): Historical aspects, present situation and forward prediction. Sci Total Environ 693:133557. https://doi.org/https://doi.org/10.1016/j.scitotenv.2019.07.363

Stoffel M, Huggel C (2012) Effects of climate change on mass movements in mountain environments. Prog Phys Geogr 36:421–439. https://doi.org/10.1177/0309133312441010

Stoffel M, Tiranti D, Huggel C (2014) Climate change impacts on mass movements - Case studies from the European Alps. Sci Total Environ 493:1255–1266. https://doi.org/10.1016/j.scitotenv.2014.02.102

Témez JR (1991) Extended and improved rational method. Version of the highways administration of Spain. In: Proc. XXIV Congress. Madrid, Spain. Vol A., pp. 33-40

Témez JR (1978) Calculo hidrometeorologico de caudales máximos en pequeñas cuencas naturales. Dirección general de carreteras, Spain. 124pp, ISBN: 84-7433-040-8.(In Spanish)

Tofani V, Bicocchi G, Rossi G, et al (2017) Soil characterization for shallow landslides modeling: a case study in the Northern Apennines (Central Italy). Landslides 14:755–770. https://doi.org/10.1007/s10346-017-0809-8

Turkington T, Remaître A, Ettema J, et al (2016) Assessing debris flow activity in a changing climate. Clim Change 137:293–305. https://doi.org/10.1007/s10584-016-1657-6

USDA (1986) Urban hydrology for small watersheds. Technical release 55.National Resources Conservation Service. National Resources Conservation Service

USDA (2007) National Engineering Handbook: Part 630 - Chapter 7: Hydrologic Soil Groups. National Resources Conservation Service

Van Beek LPHH, Van Asch TW. WJ (2004) Regional Assessment of the Effects of Land-Use Change on Landslide Hazard By Means of Physically Based Modelling. Nat Hazards 31:289–

304. https://doi.org/10.1023/B:NHAZ.0000020267.39691.39

Vanacker V, Vanderschaeghe M, Govers G, et al (2003) Linking hydrological, infinite slope stability and land-use change models through GIS for assessing the impact of deforestation on slope stability in high Andean watersheds. Geomorphology 52:299–315. https://doi.org/https://doi.org/10.1016/S0169-555X(02)00263-5

Victoriano A, García-Silvestre M, Furdada G, Bordonau J (2016) Long-term entrenchment and consequences for present flood hazard in the Garona River (Val d'Aran, Central Pyrenees, Spain). Nat Hazards Earth Syst Sci 16:2055–2070. https://doi.org/10.5194/nhess-16-2055-2016

Woodward D, Hawkins R, Hjelmfelt A, et al (2002) Curve number method: Origins, applications and limitations. In: US Geological Survey Advisory Committee on Water Information–Second Federal Interagency Hydrologic Modeling Conference. July 28-August 1, Las Vegas, Nevada

Yu B (1998) Theoretical Justification of SCS Method for Runoff Estimation. J Irrig Drain Eng 124:306–310. https://doi.org/10.1061/(asce)0733-9437(1998)124:6(306)